

# A Comprehensive Study on the Effect of ZnO and ZnAl<sub>2</sub>O<sub>4</sub> Nanoparticles on the Mechanical Properties of Epoxy Coating: Tensile and Hardness

Abeer Shmait<sup>1</sup>, Nour El Ghouch<sup>1</sup>, J. Al Boukhari<sup>2</sup>, A. M. Abdel-Gaber<sup>3</sup> & R. Awad<sup>2</sup>

<sup>1</sup> Department of Chemistry, Faculty of Science, Beirut Arab University, PO Box 11-5020 Riad El Solh, 1107 2809, Beirut, Lebanon

<sup>2</sup> Department of Physics, Faculty of Science, Beirut Arab University, PO Box 11-5020 Riad El Solh, 1107 2809, Beirut, Lebanon

<sup>3</sup> Department of Chemistry, Faculty of Science, Alexandria University, Ibrahimia, PO Box 426, Alexandria 21321, Egypt

Correspondence: J. Al Boukhari, Department of Physics, Faculty of Science, Beirut Arab University, PO Box 11-5020 Riad El Solh, 1107 2809, Beirut, Lebanon.

Received: August 24, 2021

Accepted: September 18, 2021

Online Published: September 22, 2021

doi:10.5539/mas.v15n5p45

URL: <https://doi.org/10.5539/mas.v15n5p45>

## Abstract

ZnO and ZnAl<sub>2</sub>O<sub>4</sub> nanoparticles (NPs) were successfully prepared by the co-precipitation method and characterized by x-ray powder diffraction, transmission electron microscopy, and Fourier transform infrared spectroscopy. The prepared NPs were incorporated into epoxy (EP) coating with mass ratios 200 – 800 mg/kg of ZnO NPs/EP and ZnAl<sub>2</sub>O<sub>4</sub> NPs /EP. The prepared coatings were characterized by scanning electron microscopy and Fourier transform infrared spectroscopy, and their mechanical properties were investigated, at room temperature, after 5, 10, 15, and 20 days of preparation. Tensile tests showed an improvement in the tensile properties, with the best improvement in ultimate tensile strength (93.2%) for 800 mg/kg ZnAl<sub>2</sub>O<sub>4</sub> NPs/EP coating after 15 days of preparation. The ZnO NPs/EP and ZnAl<sub>2</sub>O<sub>4</sub> NPs/EP coatings exhibited noticeable sensitivity to the stretching rate. Vickers microhardness ( $H_v$ ) investigations showed normal indentation size effect behavior for all the samples. The best improvement in  $H_v$  was attained after 5 days of preparation, for all coatings, with the best improvement (9.15%) for 700 mg/kg ZnO NPs/EP.

**Keywords:** Epoxy, mechanical properties, polymer coatings, ZnAl<sub>2</sub>O<sub>4</sub> nanoparticles, ZnO nanoparticles

## 1. Introduction

Industrial interest in epoxy (EP) originates from its vast properties, including high chemical resistance, simple processability, good adhesion to heterogeneous materials, and excellent electrical insulation (Ma et al., 2018; Samad et al., 2018). Such remarkable properties have made EP a material of choice in the marine, automotive, construction, and aircraft industries (Adesina et al., 2020; Yazman & Samancı, 2019). The curing of EP resin can be induced by heat or accelerated by adding curing agents (hardeners) (Baghdadi et al., 2020). However, when cured, EP resin tends to become very brittle with low impact resistance and toughness. This reduction in the mechanical properties of EP is due to the high cross-link density of the formed EP polymer (Baghdadi et al., 2020; M. Wu et al., 2020). Epoxies (EPs) are commonly chosen as organic coatings for protecting metals, mainly against corrosion (Samad et al., 2018; Wang et al., 2019; Yu et al., 2020). Nonetheless, the low mechanical properties of EPs make them fail on extended exposure to the environment (Samad et al., 2018).

Recently, several researchers have studied the effect of the incorporation of inorganic nanoparticles into EP resin in enhancing their tensile properties (e.g., Young's modulus, tensile strength, elongation, yield strength, yield point, and elastic limit (Rahman & Zhafer Firdaus Syed Putra, 2019)) and hardness. SiO<sub>2</sub> nanoparticles, used by Xiao *et al.* (Xiao et al., 2018) as fillers in EP resin, were effective in improving the tensile strength, flexural strength, and elastic modulus of the EP resin. Bazrgari *et al.* (Bazrgari et al., 2018) found that introducing Al<sub>2</sub>O<sub>3</sub> nanoparticles into EP resin has increased the bending strength and impact strength of EP. Moreover, Kumar *et al.* (Kumar et al., 2016) showed that TiO<sub>2</sub> nanoparticles' dispersion in EP resin has enhanced its tensile strength and failure energy. Furthermore, the introduction of AgO nanoparticles into EP could improve their mechanical

properties, as reported by Shen *et al.* (Shen *et al.*, 2021). The improvements in the mechanical properties of EP resin were attributed to the dispersion of the fine particles in the resin, which can fill cavities and cause crack deflection, crack bowing, and crack bridging. Additionally, nanoparticles are apt to occupy tiny hole defects formed from local shrinkage during the curing process of the resin and act as a bridge interconnecting more molecules (Nguyen *et al.*, 2016; Shi *et al.*, 2009).

Among inorganic metal oxides, zinc oxide nanoparticles (ZnO NPs) have acquired a marked interest in the past few years due to their interesting properties such as their excellent physical and chemical stability, low toxicity, low cost, besides their large surface area and high surface energy (Mahamuni *et al.*, 2019; Xu *et al.*, 2019). ZnO NPs are utilized in a wide variety of applications, including medicine, photoelectric materials, sensors, and coatings (Y. Wu *et al.*, 2020). Also, nano-zinc aluminate spinel has attracted great interest due to its desirable properties, including high chemical and thermal stability, high mechanical resistance, low surface acidity (Suwanboon *et al.*, 2020; Tian *et al.*, 2020), and excellent optical properties (Han, 2017; Stringhini *et al.*, 2014; Yang *et al.*, 2017). Consequently, zinc aluminate ( $\text{ZnAl}_2\text{O}_4$ ) is widely used in ceramics, catalysts, and optics industries (Han, 2017; Yang *et al.*, 2017). Many studies have reported the effect of the incorporation of ZnO and  $\text{ZnAl}_2\text{O}_4$  nanoparticles into several polymers. Liu *et al.* (X. Liu *et al.*, 2019) showed that ZnO NPs have improved the mechanical strength of PVA/xylan composite films. Alsayed *et al.* (Alsayed *et al.*, 2020) found that the values of the ultimate tensile strength and the yield stress were enhanced with the incorporation of ZnO NPs into high-density polyethylene (HDPE) polymer. Moreover, the Vickers microhardness number was improved in HDPE/ZnO composites. Devaraju *et al.* (Devaraju *et al.*, 2020) investigated the tensile, impact, and flexural properties of polymer composite material using NaOH treated palm fibers and general EP resin as matrix, with and without ZnO NPs. The results showed that the incorporation of ZnO NPs has improved the mechanical properties of the palm/EP. Moreover, zinc aluminate nanoparticles ( $\text{ZnAl}_2\text{O}_4$  NPs) added to polyurethane were found effective in acting as a cool coating on concrete cement slabs (Sameera *et al.*, 2019).

Additionally, several research papers have discussed the effect of ZnO NPs on the mechanical properties of different coatings. ZnO NPs added into acrylic coating (Vu *et al.*, 2021), polyurethane acrylate coating (Ariffin *et al.*, 2020), and alkyd coating (Sturdy *et al.*, 2020) showed an improvement in the mechanical properties of the coatings. To our knowledge, the effect of  $\text{ZnAl}_2\text{O}_4$  NPs on the mechanical properties of epoxy coating has not been previously studied. Therefore, this article will aim at studying the effect of  $\text{ZnAl}_2\text{O}_4$  NPs on the mechanical properties of EP coating. The high surface area of the  $\text{ZnAl}_2\text{O}_4$  NPs, used as fillers in the EP matrix, enhances EP mechanical properties through a more efficient load transfer mechanism. Moreover, a comparative study between ZnO and  $\text{ZnAl}_2\text{O}_4$  nanoparticles' addition and time effect on the mechanical properties of EP coating is conducted to find out the nanoparticles that provide the best mechanical properties.

In this work, we study the nanoparticles' addition and time effect on the mechanical properties of EP coating. ZnO NPs and  $\text{ZnAl}_2\text{O}_4$  NPs were synthesized via the co-precipitation method. The synthesized nanoparticles were characterized by X-ray powder diffraction (XRD), transmission electron microscopy (TEM), and Fourier transform infrared spectroscopy (FTIR). The prepared nanoparticles were incorporated into EP coating, with different mass ratios of 200, 300, 700, and 800 mg/kg of nanoparticles/coating. Moreover, the prepared coating samples were characterized by scanning electron microscopy (SEM) and FTIR. The effect of ZnO and  $\text{ZnAl}_2\text{O}_4$  nanoparticles on the tensile properties and the microhardness of EP coatings were investigated after 5, 10, 15, and 20 days of preparation. This work is organized in the present paper as follows: Sect. 2 presents the details of the preparation technique. Then, Sect. 3 illustrates the obtained results and their accompanying discussions. Finally, Sect. 4 summarizes the conclusions.

## 2. Experimental Procedures

### 2.1 Synthesis and Characterization of Zinc Oxide and Zinc Aluminate Nanoparticles

ZnO and  $\text{ZnAl}_2\text{O}_4$  nanoparticles were prepared via the co-precipitation method. The detailed synthesis and the characterization of the ZnO NPs were reported in our previous work (Shmait *et al.*, n.d.). As for the synthesis of the  $\text{ZnAl}_2\text{O}_4$  NPs, zinc chloride ( $\text{ZnCl}_2$ ,  $\geq 98\%$ , Sigma Aldrich), aluminum chloride anhydrous ( $\text{AlCl}_3$ ,  $\geq 98\%$ , Sigma Aldrich), and sodium hydroxide ( $\text{NaOH}$ ,  $\geq 98\%$ , Alpha Chemika) were used as precursors. Firstly, aqueous solutions of 1 M  $\text{ZnCl}_2$  and 1 M  $\text{AlCl}_3$  were prepared, then mixed and stirred to obtain a uniform solution. Afterward, 1 M NaOH solution was added dropwise, while stirring, until the pH of the mixture became 12. The resulting mixture was then heated at  $80^\circ\text{C}$  for 6 hours with continuous stirring. After cooling, filtration was performed and the solid was washed with distilled water until the pH of the filtrate reached 7. Thereafter, the wet solid was dried in a box furnace at  $100^\circ\text{C}$  for 18 hours. Eventually, the dried solid was ground and calcined at  $550^\circ\text{C}$  for 4 hours. The XRD pattern of the synthesized  $\text{ZnAl}_2\text{O}_4$  NPs was obtained using Bruker D8 Focus

powder diffractometer with Cu-K $\alpha$  radiation ( $\lambda=1.54056 \text{ \AA}$ ), in the range of  $20^\circ \leq 2\theta \leq 80^\circ$ , to confirm the phase formation and the purity of the prepared ZnAl $_2$ O $_4$  NPs. TEM was implemented to study morphology and the particle size of the ZnAl $_2$ O $_4$  NPs using JEM 100CX operated at 80 kV. FTIR analysis was carried out to identify the chemical bonds and the composition of the tested samples by Nicolet iS5 FTIR spectrometer in the spectral region between 4000 and 400 cm $^{-1}$ , at room temperature.

## 2.2 Preparation of Epoxy Coatings for Tensile and Microhardness Tests

The EP resin (Epichlorohydrin + Bisphenol A) and its hardener (Cycloaliphatic polyamine), shown in Figures 1 (a) and (b) (Nikolic et al., 2010; Wetzel et al., 2003), respectively, were provided by Tinol Industries - Lebanon. For all EP coatings preparations, the mass ratio of the EP resin to its hardener was 2:1. The neat EP coating was prepared by stirring EP resin with its hardener for 30 minutes. To prepare EP coatings containing ZnO NPs (ZnO NPs/EP), the required mass of the ZnO NPs was stirred with the EP resin for 10 minutes. This was followed by adding the hardener and all components were stirred for 20 minutes. Different ZnO NPs/EP coatings were prepared with concentrations of nanoparticles/(EP+hardener) of 200, 300, 700, and 800 mg/kg. The same procedure was followed in preparing EP coatings containing ZnAl $_2$ O $_4$  NPs (ZnAl $_2$ O $_4$  NPs /EP) with the same concentrations.

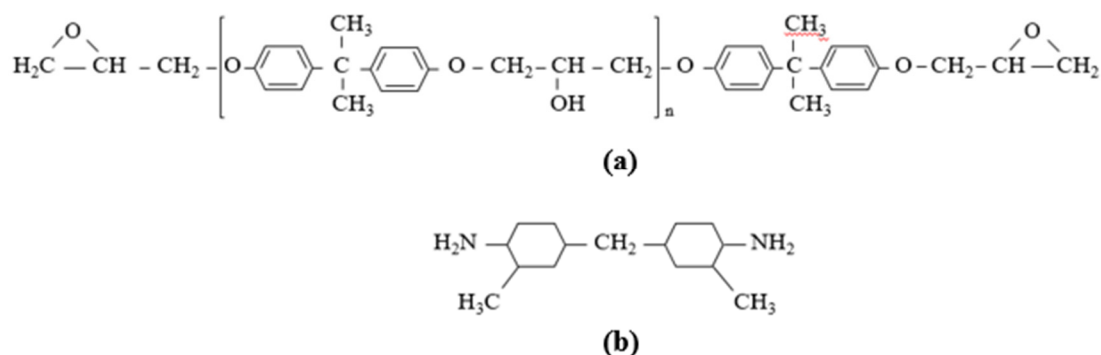


Figure 1. Chemical structure of (a) EP resin and (b) hardener

The prepared EP coatings, with and without nanoparticles, were poured into molds, and left for 5, 10, 15, and 20 days, to form films to perform the tensile and microhardness tests. The mean thickness of each of the dry films was  $500 \pm 50 \mu\text{m}$ . The surface morphology of the coating samples was characterized by a JEOL scanning electron microscope (JSM-5300). FTIR analysis of the coatings was carried out by Nicolet iS5 FTIR spectrometer in the spectral region between 4 000 and 400 cm $^{-1}$ , at room temperature. Tensile tests were performed, using ESM303 Tensile Tester (Mark-10), for films cut into dog bone specimens having 0.9 cm width, 8 cm gauge length, and 14 cm overall length. Microhardness measurements were performed using a digital Vickers microhardness tester (SIOMM model, MHVD-1000IS).

## 3. Results and Discussions

### 3.1 Nanoparticles Characterization

Figures 2 (a) and (b) show the XRD patterns of the prepared ZnO NPs and ZnAl $_2$ O $_4$  NPs, respectively. The sharp peaks reflect the crystallinity of the prepared nanoparticles (El-Fadl et al., 2019). Figure 2 (a) peaks have been indexed to the wurtzite structure of ZnO having a hexagonal phase (Babu et al., 2019; Vijayakumar et al., 2020). Moreover, the absence of extra peaks in the ZnO NPs pattern ensures the high purity of the prepared nanoparticles, which is confirmed by implementing a refinement to the XRD pattern, performed on the MAUD program and shown in Figure 2 (c). On the other hand, the formation of face-centered cubic spinel structure of ZnAl $_2$ O $_4$  is confirmed by the presence of the diffraction peaks located at  $31.26^\circ$ ,  $36.97^\circ$ ,  $44.97^\circ$ ,  $49.2^\circ$ ,  $55.92^\circ$ ,  $59.43^\circ$ ,  $65.37^\circ$ ,  $74.2^\circ$ , and  $77.5^\circ$ , which correspond to the planes of (220), (311), (400), (331), (422), (511), (440), (620), and (533), respectively, as shown in Figure 2 (b) (Xing et al., 2020). However, the appearance of additional peaks in the ZnAl $_2$ O $_4$  XRD pattern indicates the presence of an impurity phase, mainly attributed to the formation of zinc oxide (Xing et al., 2020). This is verified by the refinement to the XRD pattern, as seen in Figure 2 (d), where 88.2 and 11.8% of ZnAl $_2$ O $_4$  and ZnO phases, respectively, were obtained. The weighted profile R-factor ( $R_{wp}$ ), expected R-factor ( $R_{exp}$ ), and the goodness of the fit ( $\chi^2$ ) are shown in Figures 2 (c) and (d). The lattice parameters, obtained from the Rietveld refinement (Table 1), are found agreeable with that reported in the previous literature ( $a = 3.25$  and  $c = 5.21 \text{ \AA}$  for ZnO NPs,  $a = 8.09 \text{ \AA}$  for ZnAl $_2$ O $_4$  NPs (Tangcharoen et al.,

2019; Zak et al., 2011)). Moreover, the lattice parameters of the prepared ZnO nanoparticles are found larger than that of their bulk counterpart ( $a = 3.12$  and  $c = 5.05$  Å (Gallegos et al., 2019)), demonstrating that the lattice parameters have increased in the nanoscale (Fukuhara, 2003), subsequently, inducing microstrain in the crystalline lattice. Microstrains, which are very common in nanoparticles, are mainly caused by the high surface energy of the nanoparticles. A large fraction of the surface atoms in materials at the nanoscale are under-coordinated and present a bond order deficiency, as compared to their bulk equivalent form (Alsaad et al., 2020; Andrade et al., 2017). The obtained microstrain ( $\epsilon$ ) values for ZnO and ZnAl<sub>2</sub>O<sub>4</sub> nanoparticles are listed in Table 1. The microstrain value of the synthesized ZnO NPs is quite similar to that reported by Almeida *et al.* for ZnO NPs, prepared by the sol-gel method (Lopes de Almeida et al., 2021). However, a lower microstrain value for ZnAl<sub>2</sub>O<sub>4</sub> NPs is obtained in this work, as compared to that reported by El-Fadl *et al.* (El-Fadl et al., 2019), for ZnAl<sub>2</sub>O<sub>4</sub> NPs prepared via microwave combustion method. A lower microstrain reflects a reduction in lattice defect along the grain boundaries (Shaban et al., 2020).

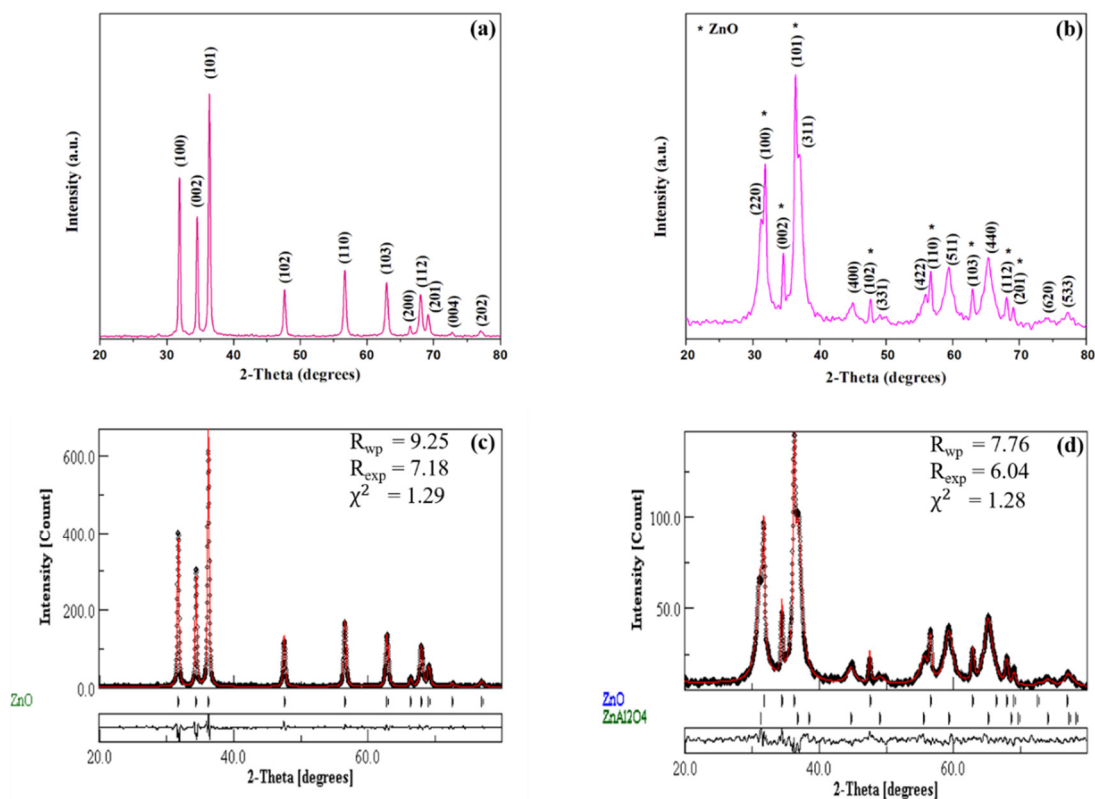


Figure 2. XRD pattern of (a) ZnO NPs and (b) ZnAl<sub>2</sub>O<sub>4</sub> NPs. Rietveld refinement of (c) ZnO NPs and (d) ZnAl<sub>2</sub>O<sub>4</sub>

Table 1. Structural parameters of ZnO and ZnAl<sub>2</sub>O<sub>4</sub> nanoparticles

	ZnO	ZnAl <sub>2</sub> O <sub>4</sub>
<b>a</b> (Å)	$3.25 \pm 1.0 \times 10^{-4}$	$8.09 \pm 4.3 \times 10^{-4}$
<b>c</b> (Å)	$5.21 \pm 1.8 \times 10^{-4}$	-
<b>D</b> (nm)	$23.84 \pm 0.31$	$6.61 \pm 0.31$
<b><math>\epsilon</math></b> ( $\times 10^{-3}$ )	$1.52 \pm 0.02$	$1.93 \pm 0.23$
<b><math>\rho_x</math></b> (kg/m <sup>3</sup> )	$11312.9 \pm 1.13$	$4587.4 \pm 0.74$
<b><math>\delta</math></b> ( $\times 10^{15}$ m <sup>-2</sup> )	$1.76 \pm 0.04$	$22.90 \pm 2.10$
<b>S</b> ( $\times 10^4$ m <sup>2</sup> /kg)	$2.22 \pm 0.03$	$19.78 \pm 0.92$

The average crystallite size ( $D$ ) of the synthesized nanoparticles was calculated using Debye - Scherrer equation (Al Boukhari et al., 2019; Ghouch et al., 2019):

$$D = \frac{0.9\lambda}{\beta \cos\theta} \quad (1)$$

where 0.9 is Scherrer's constant,  $\lambda$  is the X-ray wavelength,  $\beta$  is the full width at half maximum height (in radians), and  $2\theta$  is the diffraction angle. The crystallite size of the ZnO and ZnAl<sub>2</sub>O<sub>4</sub> nanoparticles was found to be 23.84 nm and 6.61 nm, respectively.

The x-ray density ( $\rho_x$ ), the dislocation density ( $\delta$ ), and the specific surface area ( $S$ ) were calculated using the following equations (El-Fadl et al., 2019; Kamareddine et al., 2020):

$$\rho_x = \frac{nM}{N_A V} \quad (2)$$

$$\delta = \frac{1}{D^2} \quad (3)$$

$$S = \frac{6}{\rho_x D} \quad (4)$$

where  $n$ ,  $M$ ,  $N_A$ , and  $V$  refer to the number of atoms per unit cell (4 for ZnO (Galsin, 2019) and 8 for ZnAl<sub>2</sub>O<sub>4</sub> (El-Fadl et al., 2019)), molecular weight, Avogadro's number, and the unit cell volume. The results, listed in Table 1, show that the specific surface area of ZnAl<sub>2</sub>O<sub>4</sub> NPs is greater than that of ZnO NPs. This helps in many applications as improving the mechanical properties of EP coatings upon the incorporation of the ZnAl<sub>2</sub>O<sub>4</sub> NPs.

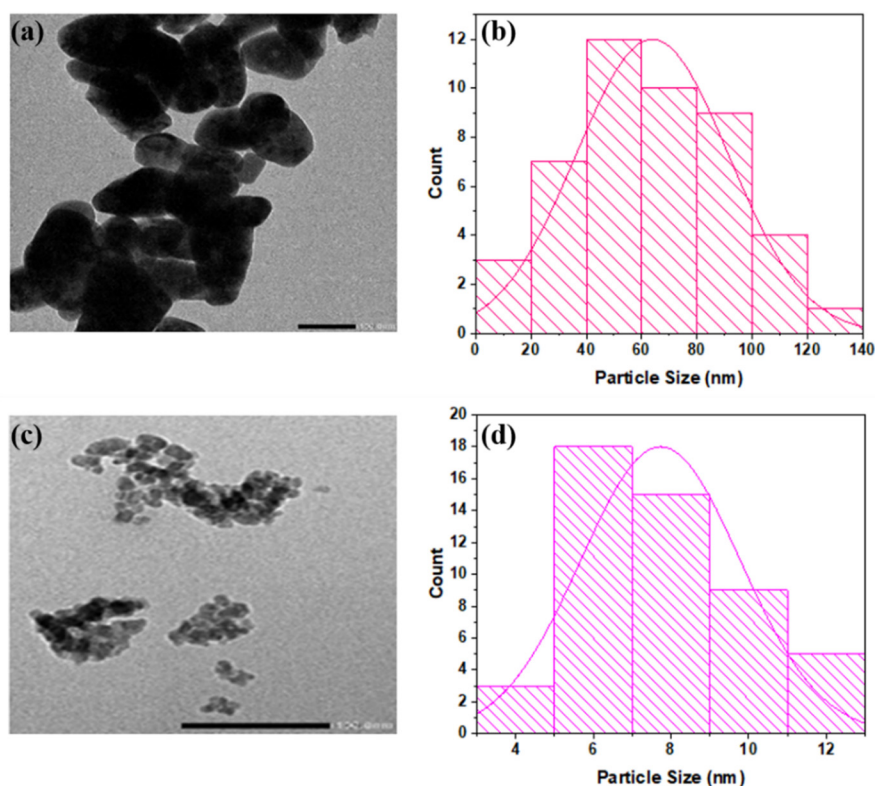


Figure 3. ZnO NPs (a) TEM image and (b) particle size histogram. ZnAl<sub>2</sub>O<sub>4</sub> NPs (c) TEM image and (d) particle size histogram

Figures 3 (a, b) and (c, d) represent the TEM image and the corresponding particle size distribution histogram for ZnO NPs and ZnAl<sub>2</sub>O<sub>4</sub> NPs, respectively. The TEM image of the ZnO NPs, displayed in Figure 3 (a), shows slightly agglomerated, homogeneous particles with distorted hexagonal morphology. On the other hand, the TEM image of ZnAl<sub>2</sub>O<sub>4</sub> NPs shows agglomerated nanoparticles exhibiting homogeneous, nearly spherical morphology, as seen in Figure 3 (c). Moreover, the histograms displayed in Figures 3 (b) and (d), obtained using the ImageJ software, show that the maximum number of particles have a particle size of 49.09 and 7.73 nm for ZnO NPs and ZnAl<sub>2</sub>O<sub>4</sub> NPs, respectively. The high surface area of the nanoparticles and the strong attractive forces between the nanoparticles lead to their aggregation (Ashraf et al., 2018). The final particle of ZnO has reached a larger size as compared to the crystallite size obtained from XRD, which confirms that the ZnO particles were formed from the combination of crystallites (Jensen et al., 2006; Kibasomba et al., 2018). The particle size of ZnO NPs larger than crystallite size was reported by Vijayakumar *et al.* (Vijayakumar et al., 2020) for ZnO NPs prepared by the co-precipitation method. Nonetheless, the particle size of ZnAl<sub>2</sub>O<sub>4</sub> is in good agreement with the crystallite size obtained from the XRD analysis. Likewise, the particle size agrees with the

crystallite size for  $\text{ZnAl}_2\text{O}_4$  prepared by Jagadeeshwaran *et al.* (Jagadeeshwaran & Murugaraj, 2019) by the co-precipitation method.

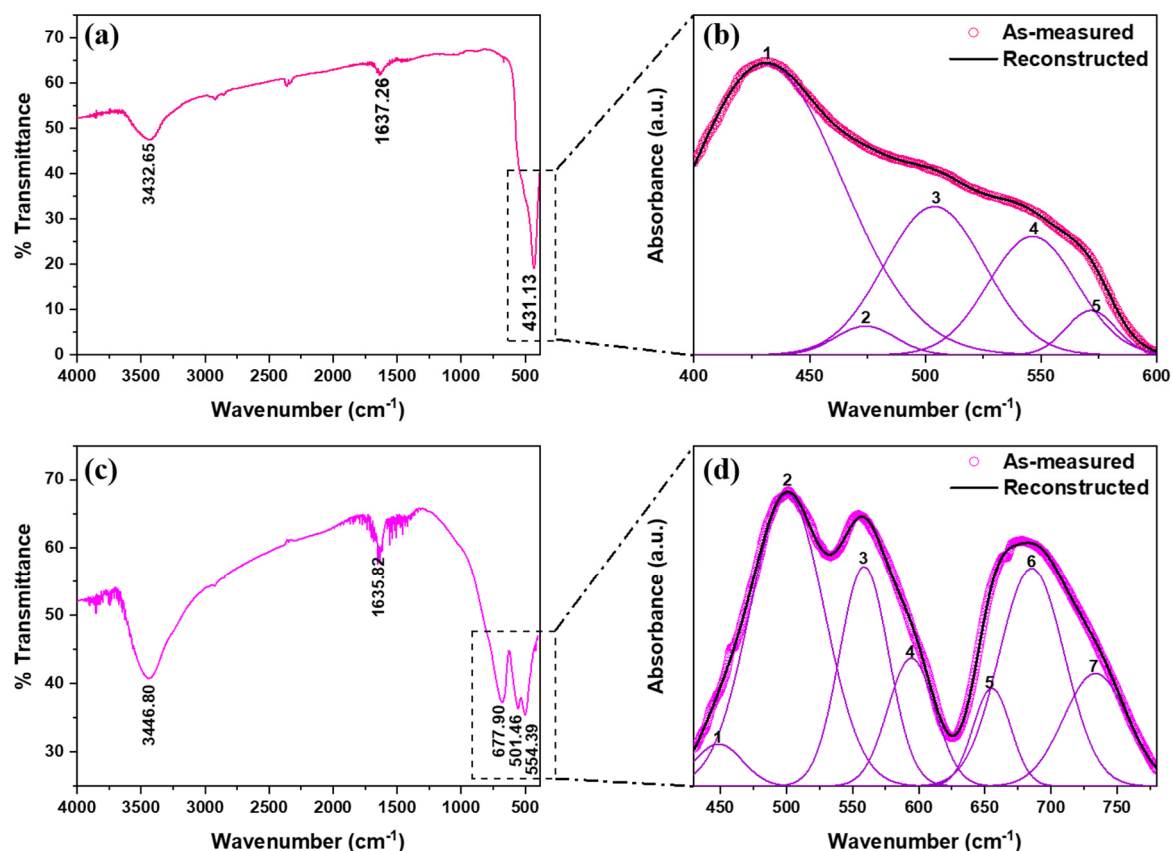


Figure 4. ZnO NPs (a) FTIR spectrum and (b) FTIR Deconvolution.  $\text{ZnAl}_2\text{O}_4$  NPs (c) FTIR spectrum and (d) FTIR Deconvolution

Figures 4 (a, b) and (c, d) depict the FTIR spectrum and FTIR deconvolution graphs of the synthesized ZnO NPs and  $\text{ZnAl}_2\text{O}_4$  NPs, respectively. The deconvolution parameters of ZnO NPs and  $\text{ZnAl}_2\text{O}_4$  NPs are given in Table 2. The strong band appearing at  $431.13\text{ cm}^{-1}$  in Figure 4 (a) corresponds to Zn-O stretching vibration mode confirming the successful preparation of ZnO NPs. As seen in Figure 4 (c), a broad absorption band appears at  $3446.80\text{ cm}^{-1}$ , representing the O-H stretching vibrations. Also, a weak band appears at  $1635.82\text{ cm}^{-1}$ , corresponding to H-O-H bending vibrations (Naik *et al.*, 2020). These two bands indicate the small water content in the  $\text{ZnAl}_2\text{O}_4$  NPs samples (Hassan *et al.*, 2020; Subhasree *et al.*, 2020). There is no peak in the range  $1028 - 1157\text{ cm}^{-1}$ , which confirms the absence of Al-OH bending vibrations (Bayal & Jeevanandam, 2012). Moreover, the three peaks observed at  $677.90$ ,  $554.39$ , and  $501.46\text{ cm}^{-1}$  indicate the formation of the spinel-type structure (Guo *et al.*, 2017). Similar results were obtained with Belyaev *et al.* (Belyaev *et al.*, 2019). The spinel structures exhibit stretching bands in the  $500-900\text{ cm}^{-1}$  range, which are associated with metal-oxygen, aluminum-oxygen, and metal-oxygen-aluminum stretching vibrations (Sameera *et al.*, 2019; Yuvasravana *et al.*, 2017). Figures 4 (b) and (d) show the deconvolution, by multiple peak fitting using the Gaussian function, of the characteristic peaks of ZnO and  $\text{ZnAl}_2\text{O}_4$  nanoparticles, respectively. For ZnO NPs, Figure 4 (b), the strong peak (1) observed at  $430.7\text{ cm}^{-1}$  reveals the ZnO NPs vibrational properties (Zheng *et al.*, 2007). Peak (3) at  $503.9\text{ cm}^{-1}$  can be assigned to oxygen deficiency in the ZnO NPs (Fernández-Pérez *et al.*, 2017; Multian *et al.*, 2017). Peaks (2), (4), and (5) at  $474.07$ ,  $546.4$ , and  $571.6\text{ cm}^{-1}$  may be associated with local vibrational modes of impurities or defects (Muñoz-Hernández *et al.*, 2009). In Figure 4 (d), peak (2) component represents spinel  $\text{ZnAl}_2\text{O}_4$ . Peaks (1) and (7), at  $448.6$  and  $733.7\text{ cm}^{-1}$ , correspond to tetrahedral  $\text{ZnO}_4$  (Jain *et al.*, 2019) and tetrahedral  $\text{AlO}_4$  coordination (Tsai *et al.*, 2013), respectively. Peaks (3), (4), (5), and (6) may be associated with deformation in the spinel structure (Staszak *et al.*, 2010).

Table 2. Deconvolution parameters of the infrared spectra of ZnO and ZnAl<sub>2</sub>O<sub>4</sub> nanoparticles

		<b>Center (cm<sup>-1</sup>)</b>	<b>Intensity (a.u)</b>	<b>HWHM (cm<sup>-1</sup>)</b>
<b>ZnO NPs</b>	1	430.7 ± 0.27	42.8 ± 0.11	38.8 ± 0.29
	2	474.1 ± 1.34	4.2 ± 2.46	15.3 ± 1.99
	3	503.9 ± 0.71	21.8 ± 1.29	25.6 ± 3.53
	4	546.3 ± 2.11	17.4 ± 1.78	22.5 ± 0.82
	5	571.6 ± 0.28	6.5 ± 0.59	12.6 ± 0.43
<b>ZnAl<sub>2</sub>O<sub>4</sub> NPs</b>	1	448.6 ± 1.22	1.6 ± 0.16	21.1 ± 1.03
	2	500.5 ± 0.18	11.1 ± 0.02	32.8 ± 0.78
	3	558.7 ± 0.63	8.3 ± 0.34	21.7 ± 0.69
	4	594.4 ± 1.20	4.8 ± 0.28	21.0 ± 0.91
	5	655.3 ± 0.24	3.7 ± 0.81	16.7 ± 0.96
	6	685.5 ± 0.89	8.3 ± 0.43	28.9 ± 2.55
	7	733.7 ± 2.48	4.3 ± 0.43	28.4 ± 0.91

### 3.2 Characterization of the Coatings

#### 3.2.1 Morphological Characterization

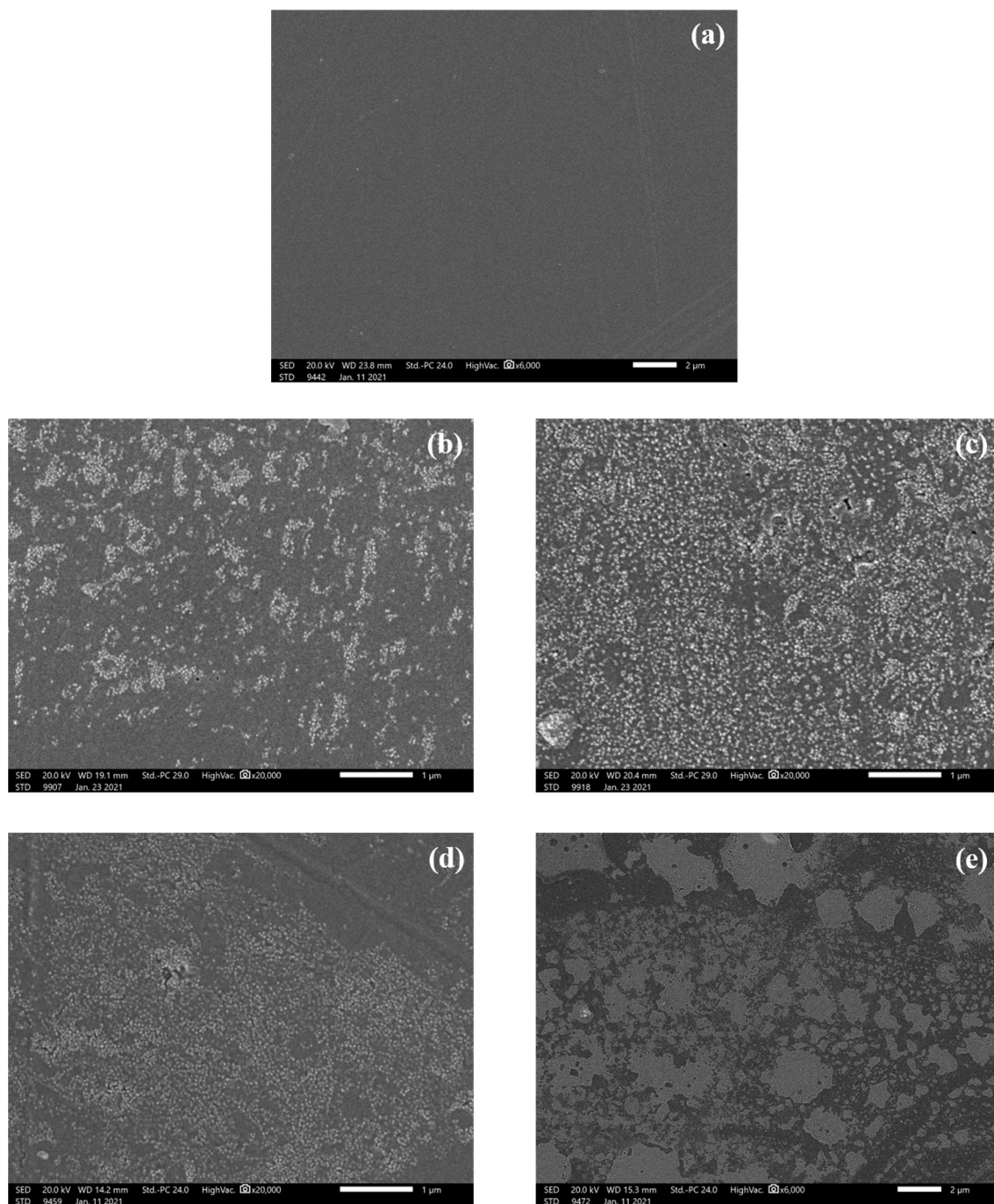


Figure 5. SEM micrographs of (a) neat EP, (b) 200 mg/kg ZnO NPs/EP, (c) 700 mg/kg ZnO NPs/EP, (d) 200 mg/kg ZnAl<sub>2</sub>O<sub>4</sub> NPs/EP, and (e) 700 mg/kg ZnAl<sub>2</sub>O<sub>4</sub> NPs/EP

SEM micrographs of neat EP, ZnO NPs/EP, and ZnAl<sub>2</sub>O<sub>4</sub> NPs/EP (200 and 700 mg/kg) coatings, are displayed in Figure 5 (a-e). Figure 5 (a) shows that neat EP coating presents a smooth surface. However, a rough surface is observed in EP coatings incorporated with ZnO or ZnAl<sub>2</sub>O<sub>4</sub> nanoparticles, as seen in Figures 5 (b) and (c) and Figures 5 (d) and (e), respectively. Surface roughness increased with the increase in the concentration of ZnO and ZnAl<sub>2</sub>O<sub>4</sub> nanoparticles in EP. Moreover, the micrographs depicted in Figure 5 (b-e), show a nearly uniform distribution of ZnO and ZnAl<sub>2</sub>O<sub>4</sub> nanoparticles in the EP matrix. Nonetheless, some agglomeration appears in the 700 mg/kg ZnO NPs/EP coating. Additionally, some nanoparticles-free spaces are observed in the ZnO NPs/EP and ZnAl<sub>2</sub>O<sub>4</sub> NPs/EP samples, as shown in Figure 5 (b-e).

### 3.2.2 Fourier Transform Infrared Spectroscopy

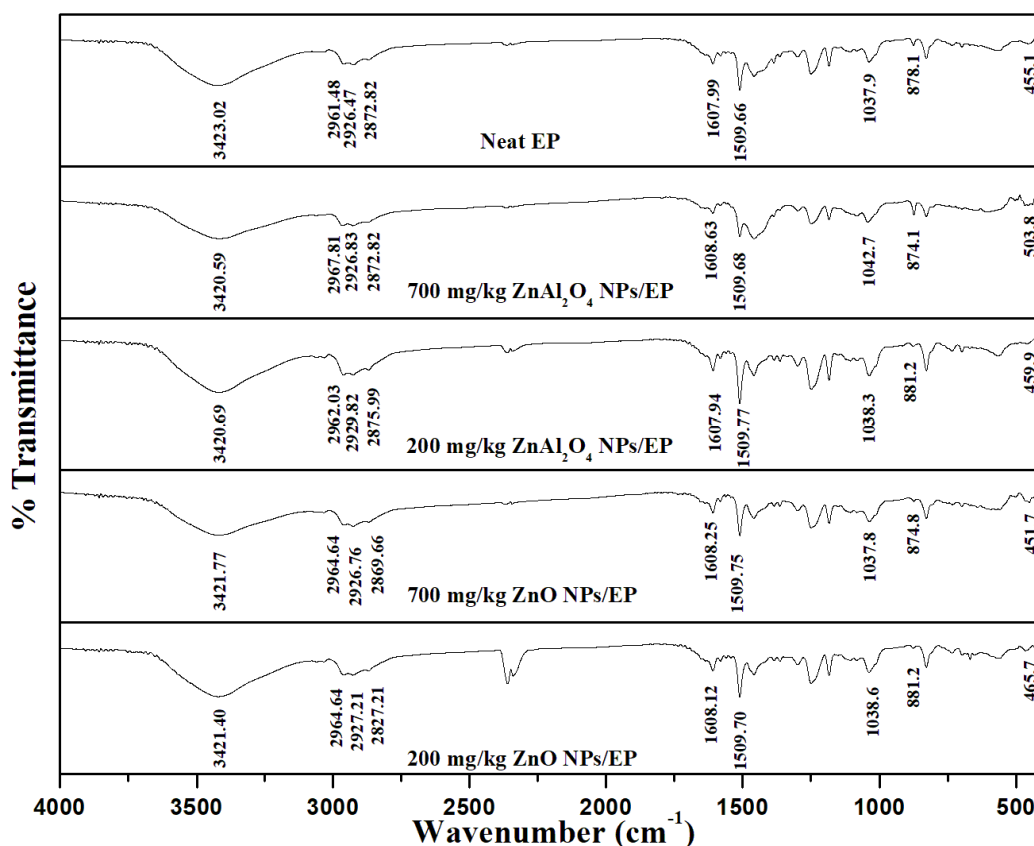


Figure 6. FTIR spectra of 200 mg/kg ZnO NPs/EP, 700 mg/kg ZnO NPs/EP, 200 mg/kg ZnAl<sub>2</sub>O<sub>4</sub> NPs/EP, 700 mg/kg ZnAl<sub>2</sub>O<sub>4</sub> NPs/EP, and Neat EP

The FTIR spectra of neat EP, ZnO NPs/EP, and ZnAl<sub>2</sub>O<sub>4</sub> NPs/EP (200 and 700 mg/kg) coatings are shown in Figure 6. The FTIR spectrum of neat EP shows a broad peak at 3 423.02 cm<sup>-1</sup>, which corresponds to the OH group. Moreover, peaks appear at 2 872.82, 2 926.47, and 2 961.48 cm<sup>-1</sup>, which correspond to C-H stretching (Ammar et al., 2016). Furthermore, peaks at 1607.99 and 1509.66 cm<sup>-1</sup> correspond to the stretching C=C and C-C of aromatic rings, respectively (Theophile, 2012). A comparison of ZnO/EP and ZnAl<sub>2</sub>O<sub>4</sub>/EP with neat EP shows similar spectra. However, the presence of ZnO and ZnAl<sub>2</sub>O<sub>4</sub> nanoparticles in EP resin resulted in peak shifts, including 455.1, 878.1, and 1 037.9 cm<sup>-1</sup>. Peak shifting in FTIR spectra upon the inclusion of ZnO nanoparticles in EP was reported by Verma *et al.* (Verma et al., 2019) and Ammar *et al.* (Ammar et al., 2016).

### 3.3 Mechanical Properties of the Coatings

#### 3.3.1 Tensile Tests

Studying the mechanical properties of materials is necessary since they help us understand the materials' behavior. As such, the tensile properties of EP coatings, with and without ZnO or ZnAl<sub>2</sub>O<sub>4</sub> nanoparticles, were investigated at room temperature, under stretching rates of 1 and 3 mm/min, after 10, 15, and 20 days of preparation.

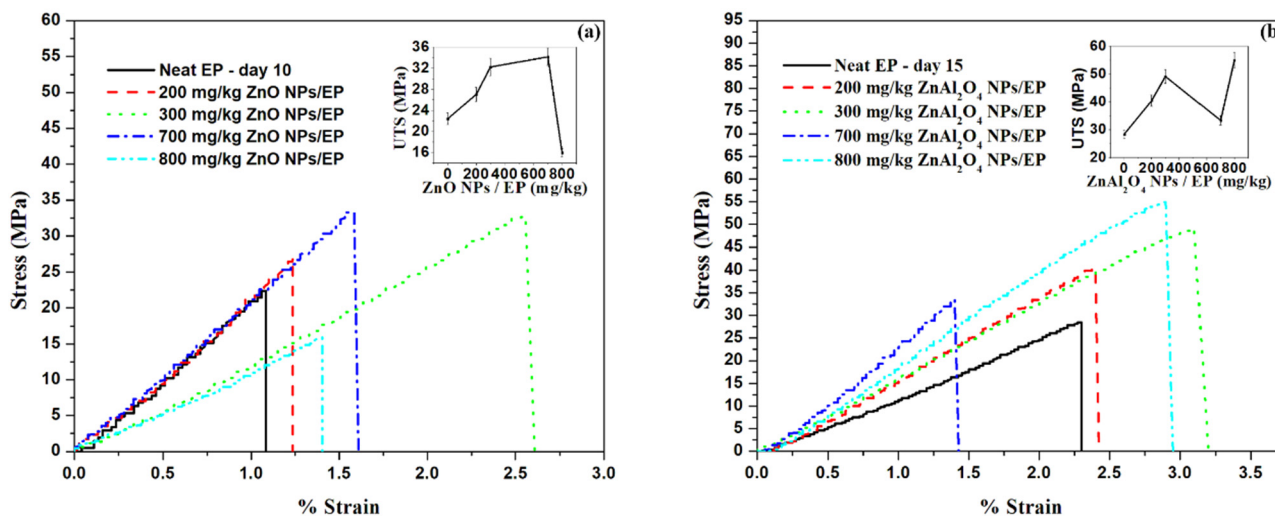


Figure 7. Stress-Strain curves for EP coatings, under stretching rate of 3 mm/min, with and without (a) ZnO NPs on day 10 and (b) ZnAl<sub>2</sub>O<sub>4</sub> NPs on day 15. The insets show ultimate tensile strength versus concentration for EP coatings with and without (a) ZnO NPs on day 10 and (b) ZnAl<sub>2</sub>O<sub>4</sub> NPs on day 15

Figures 7 (a) and (b) represent the typical stress-strain curves, under stretching rate of 3 mm/min, of neat EP, day 10 ZnO NPs/EP, and day 15 ZnAl<sub>2</sub>O<sub>4</sub> NPs/EP (200, 300, 700, and 800 mg/kg) coatings. The shapes of the curves show that all EP coating specimens, with and without ZnO or ZnAl<sub>2</sub>O<sub>4</sub> nanoparticles, have elastically deformed under load and then were suddenly broken; there was no transition to a plastic deformation, which implies that all specimens have indicated brittle behavior (J. Liu et al., 2020; Ünal et al., 2016). The ultimate tensile strength (UTS) of EP coating was enhanced upon the incorporation of ZnO and ZnAl<sub>2</sub>O<sub>4</sub> nanoparticles, as seen in Figures 7 (a) and (b), respectively. UTS determines the ability of a material to resist failure under longitudinal tensile stress (Saba et al., 2019; Wei et al., 2019). Thus, the ability of EP coating in resisting deformation and fracture was improved with the addition of ZnO and ZnAl<sub>2</sub>O<sub>4</sub> nanoparticles. The UTS of neat EP coating was 22.4 MPa, on day 10. As shown in Figure 7 (a) inset, an increase in the UTS of EP coating upon ZnO NPs incorporation was 20.7% with 200 mg/kg ZnO NPs/EP coating, as compared to neat EP. After that, an increase in the concentration of ZnO NPs in EP to 300 and 700 mg/kg has increased the UTS by 45.9 and 48.5%, respectively, as compared to neat EP. This increase in UTS may be attributed to the following mechanism: the fine particles of ZnO were evenly distributed in the EP resin, which makes the load transfer between the nanoparticles and the EP resin equal (Bazrgari et al., 2018; Kameswara Reddy et al., 2020). Additionally, the strong interfacial bonds between the ZnO NPs and the EP resin enhance the mechanical properties by providing an effective load transfer to the nanoparticles, which are more rigid in the EP resin (Ma et al., 2018; Yazman & Samancı, 2019). Nonetheless, with a further increase in the concentration of ZnO NPs in EP resin to 800 mg/kg, a decrease of 29.01% in the UTS of the coating, as compared to neat EP, was noticed. This may be attributed to the agglomeration of the ZnO NPs, which then become unevenly distributed in the EP resin (Kameswara Reddy et al., 2020; Wei et al., 2019; M. Wu et al., 2020; Xia et al., 2019). Furthermore, ZnO NPs agglomeration might have created micro-cracks in the EP matrix (Frigione & Lettieri, 2020). The results, presented in Figure 7 (a), are in good agreement with the SEM micrograph analysis for EP coatings, in which some agglomeration was noticed in 700 mg/kg ZnO NPs/EP coating. On the other hand, the UTS of neat EP coating was 28.4 MPa, on day 15, as seen in Figure 7 (b). The incorporation of ZnAl<sub>2</sub>O<sub>4</sub> NPs into EP resin, in concentrations of 200, 300, 700, and 800 mg/kg, has increased the UTS by 42.4, 72.8, 17.4, and 93.2%, respectively, as compared to neat EP. Likewise, this might be attributed to the uniform distribution of the ZnAl<sub>2</sub>O<sub>4</sub> NPs in EP. The 700 mg/kg ZnAl<sub>2</sub>O<sub>4</sub> NPs/EP coating was more easily ruptured than neat EP, during the tensile test. This may be attributed to the formation of irregular voids in the coating, which hinder the EP resin mobility (Alsayed et al., 2020). Generally, ZnAl<sub>2</sub>O<sub>4</sub> NPs/EP showed better enhancement in the UTS than the corresponding ZnO NPs/EP coating samples. This might be attributed to the smaller particle size of the ZnAl<sub>2</sub>O<sub>4</sub> NPs, as compared to ZnO NPs, which enhances its ability to penetrate ultra-small holes, indentations, and capillary area in the EP matrix (Nguyen et al., 2016). ZnAl<sub>2</sub>O<sub>4</sub> NPs have a higher total surface area, as confirmed in the XRD analysis, which causes a more efficient transfer of stress between the nanoparticles and the EP polymer, hence, giving better reinforcement (Fu et al., 2008; Ma et al., 2018). Additionally, an enhancement in Young's modulus and the elongation-at-break with ZnO NPs/EP and ZnAl<sub>2</sub>O<sub>4</sub> NPs/EP coating, as compared to neat EP, was observed, as shown in Figures 8 (a)

and (b). Young's modulus, determined from the slope of the linear segment in the stress-strain curve, is a measure of the stiffness of a material (Ünal et al., 2016), and the elongation-at-break represents the ability of a material to resist changes of shape without cracking (Djafari Petroudy, 2017). An increase in Young's modulus and the elongation-at-break, upon the incorporation of ZnO or ZnAl<sub>2</sub>O<sub>4</sub> nanoparticles into EP resin, has ensured an improvement in the stiffness and the toughness of the coating (Wei et al., 2019). Young's modulus and the elongation-at-break of neat EP coating, on day 15, were 1.26 GPa and 2.3%, respectively, which increased to 2.038 GPa and 2.9% with 800 mg/kg ZnAl<sub>2</sub>O<sub>4</sub> NPs/EP specimen. The 200 mg/kg ZnAl<sub>2</sub>O<sub>4</sub> NPs/EP specimen, at failure, is presented in Figure 9.

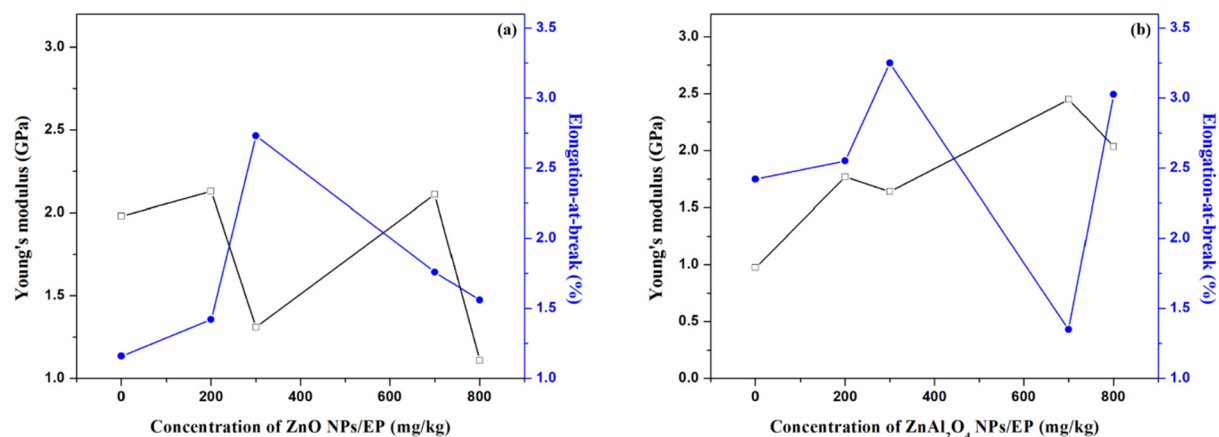


Figure 8. (a) Young's modulus and (b) elongation-at-break, under stretching rate of 3 mm/min, versus concentration of EP coating, with and without ZnO NPs on day 10 and ZnAl<sub>2</sub>O<sub>4</sub> NPs on day 15



Figure 9. Photo of 200 mg/kg ZnAl<sub>2</sub>O<sub>4</sub> NPs/EP specimen at failure

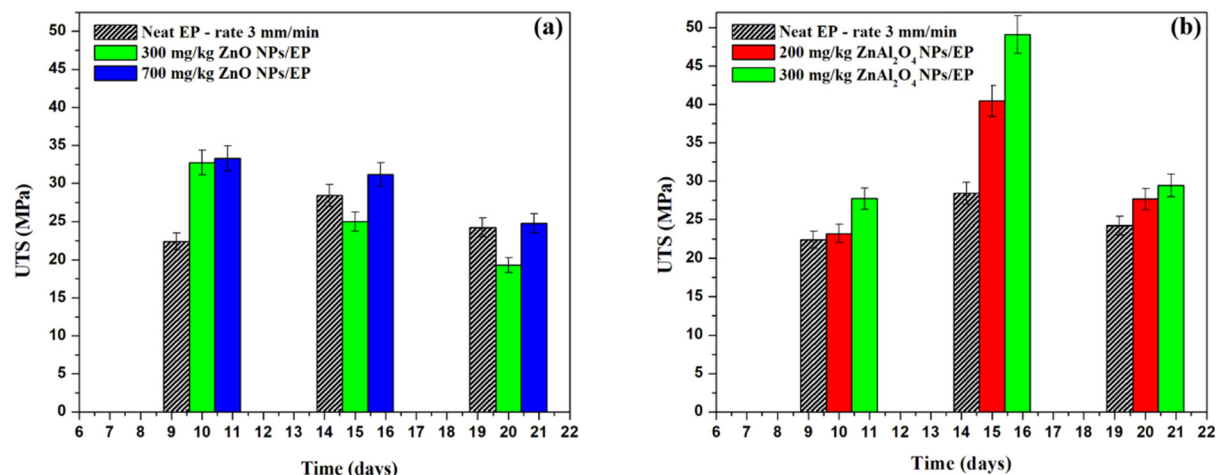


Figure 10. Ultimate tensile strength versus time of (a) neat EP, 300, and 700 mg/kg ZnO NPs/EP and (b) neat EP, 200, and 300 mg/kg ZnAl<sub>2</sub>O<sub>4</sub> NPs/EP, under stretching rate of 3 mm/min

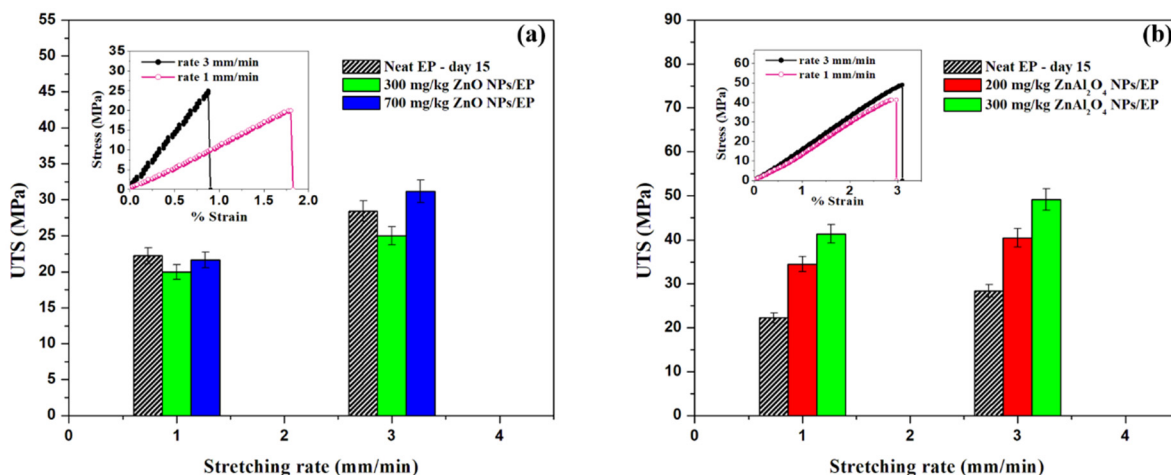


Figure 11. Ultimate tensile strength versus Stretching rate for (a) neat EP, 300, and 700 mg/kg, ZnO NPs/EP and (b) neat EP, 200, and 300 mg/kg ZnAl<sub>2</sub>O<sub>4</sub> NPs/EP, on day 15. The insets show stress-strain curves for 300 mg/kg (a) ZnO NPs/EP and (b) ZnAl<sub>2</sub>O<sub>4</sub> NPs/EP at stretching rates of 1 and 3 mm/min, on day 15

Comparison of the UTS values versus time, under a stretching rate of 3 mm/min, is shown for neat EP, ZnO NPs/EP (300 and 700 mg/kg), and ZnAl<sub>2</sub>O<sub>4</sub> NPs/EP (200 and 300 mg/kg) specimens, in Figures 10 (a) and (b). It was observed that the highest increase in the UTS of ZnO NPs/EP and ZnAl<sub>2</sub>O<sub>4</sub> NPs/EP coating was reached on days 10 and 15, respectively, then began to decrease. The decrease in the UTS of the coating samples may be attributed to environmental effects, mainly temperature and humidity (Glaskova-Kuzmina et al., 2020; Odegard & Bandyopadhyay, 2011; Savvilotidou et al., 2017). Water absorption, even at low amounts, weakens the interface between the nanoparticles and the EP matrix, which obstructs stress transfer under mechanical loads (Frigione & Lettieri, 2020). Similar results were obtained with Pattanaik *et al.* (Pattanaik et al., 2020), in which the tensile strength of fly ash-filled EP composites has decreased under a natural humid atmospheric environment. The effect of the stretching rate on the UTS of neat EP, ZnO NPs/EP (300 and 700 mg/kg), and ZnAl<sub>2</sub>O<sub>4</sub> NPs/EP (200 and 300 mg/kg) specimens, was studied for day 15 samples. The results are shown in Figures 11 (a) and (b). As noticed, when the stretching rate was decreased from 3 to 1 mm/min, the UTS of all specimens decreased. Similar results were obtained with Gurusideswar *et al.* (Gurusideswar et al., 2017) for Glass/EP composites. Thus, the UTS of neat EP, ZnO NPs/EP, and ZnAl<sub>2</sub>O<sub>4</sub> NPs/EP coatings are rate sensitive. It was found that the ZnO NPs/EP samples are more sensitive to the decrease in the stretching rate than ZnAl<sub>2</sub>O<sub>4</sub> NPs/EP. A decrease by 20.1 and 30.5% in the UTS was observed for 300 and 700 mg/kg ZnO NPs/EP, respectively, as the stretching rate was decreased from 3 to 1 mm/min. On the other hand, 14.7 and 15.8% decrease in UTS was observed for 200 and 300 mg/kg ZnAl<sub>2</sub>O<sub>4</sub> NPs/EP, respectively. The insets of Figures 11 (a) and (b) depict the stress-strain curves of 300 mg/kg ZnO NPs/EP and 300 mg/kg ZnAl<sub>2</sub>O<sub>4</sub> NPs/EP, respectively, at stretching rates of 1 and 3 mm/min, in which Young's modulus, for the two specimens, has decreased with the

decrease in the stretching rate. An increase in the stretching rate decreases the molecular mobility of the EP polymer chains, which leads to an increase in the stiffness and brittleness of the material (Gurusideswar et al., 2017).

### 3.3.2 Vickers Microhardness

At room temperature, the microhardness of EP coating samples, with and without ZnO or ZnAl<sub>2</sub>O<sub>4</sub> nanoparticles, was measured by applying Vickers pyramidal indenter after 5, 10, 15, and 20 days of preparation. Different loads varying from 0.245 to 4.90 N, at a dwell loading time of 30 seconds, were applied. For each load, three different hits at different positions on the sample's surface were applied and Vickers microhardness value was determined using the given equation (Srouf et al., 2017; Zalaoglu et al., 2017):

$$H_V = 1854.4 \frac{F}{d^2} \tag{5}$$

where  $H_V$  is Vickers microhardness (GPa),  $F$  is the applied load in (N), and  $d$  is the average of the diagonals of the indentation marks of the three hits in ( $\mu\text{m}$ ). The variation of  $H_V$  with  $F$ , after 5, 10, 15, and 20 days of preparation, for neat EP, ZnO NPs/EP, and ZnAl<sub>2</sub>O<sub>4</sub> NPs/EP (200, 300, 700 and 800 mg/kg) coating samples, is displayed in Figure 12 (a-d) and Figure 13 (a-d).

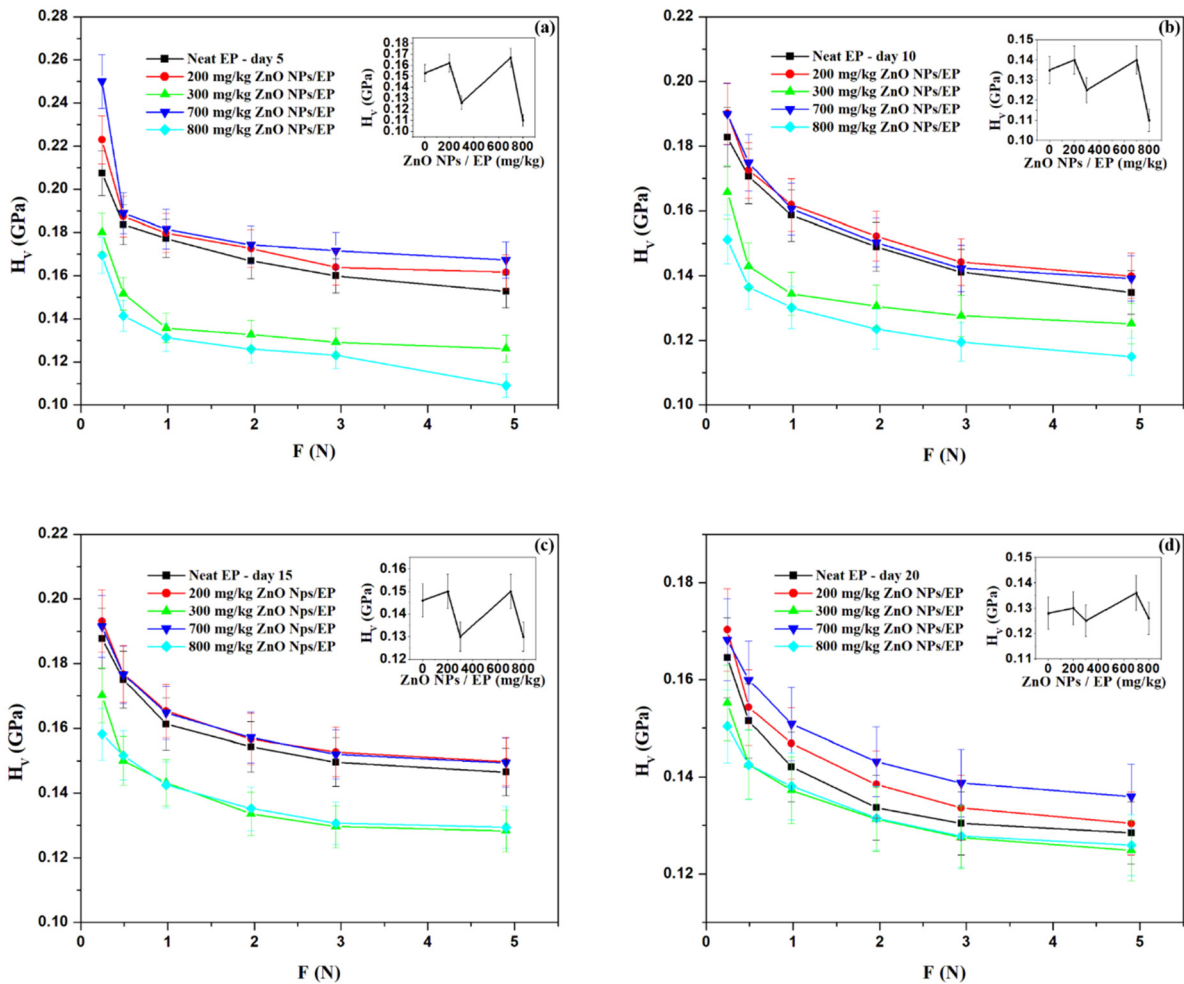


Figure 12. Microhardness  $H_V$  with applied load  $F$  for EP coatings, with and without ZnO NPs, after (a) 5, (b) 10, (c) 15, and (d) 20 days. The insets show the variation of  $H_V$ , under 4.90 N load, with the concentration of ZnO NPs in EP

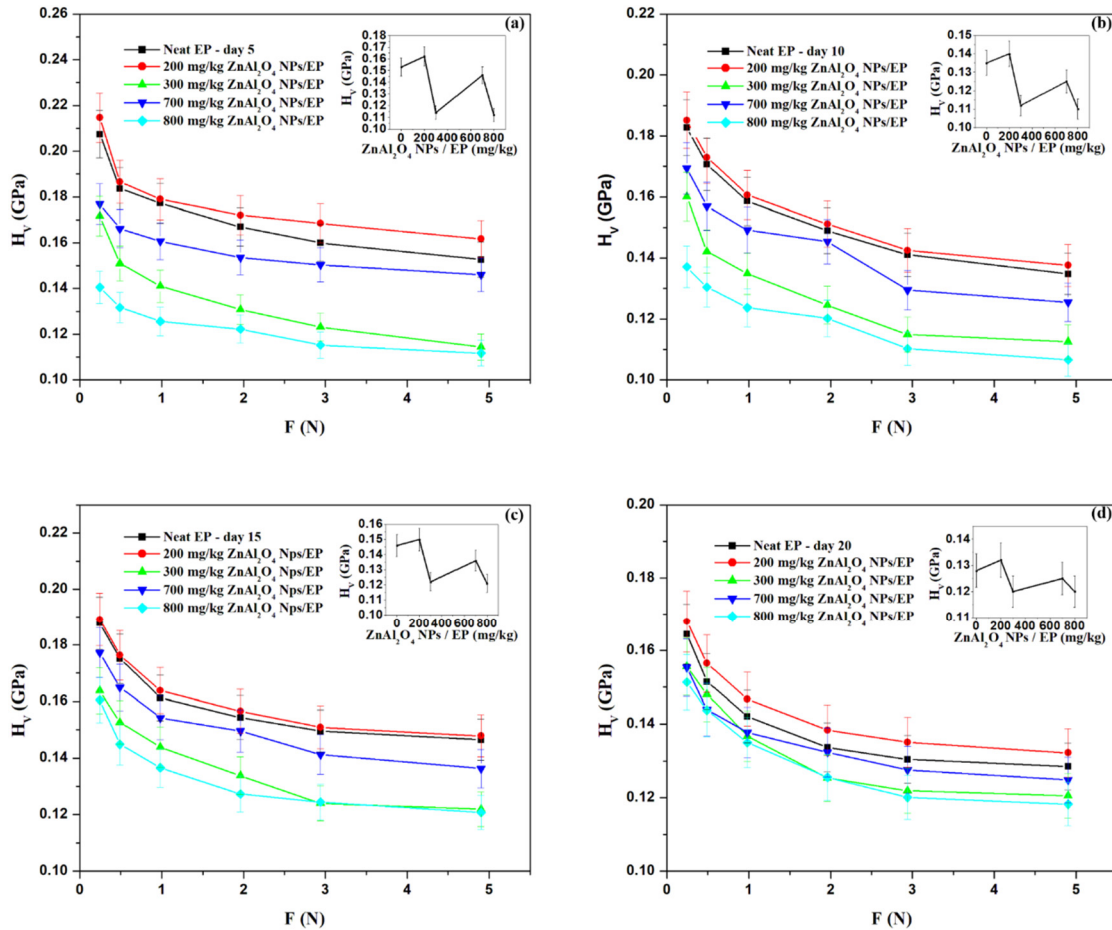


Figure 13. Microhardness  $H_v$  with applied load  $F$  for EP coatings, with and without  $ZnAl_2O_4$  NPs, after (a) 5, (b) 10, (c) 15, and (d) 20 days. The insets show the variation of  $H_v$ , under 4.90 N load, with the concentration of  $ZnAl_2O_4$  NPs in EP

It was found that for all samples, the  $H_v$  values were load-dependent, as  $H_v$  decreased non-linearly with increasing the applied load until  $F = 2.94$  N, then nearly attained saturation showing a nearly plateau region, at higher loads. This behavior is known as the normal indentation size effect (ISE) (Awad et al., 2014; Sahoo & Behera, 2019). The normal ISE behavior can be explained based on the indenter’s penetration depth. At small loads, the indenter penetrates the surface of the sample, limiting the load effect to the surface layer only. However, at higher loads, the depth of penetration increases, and then the effect of the inner layers dominates (Awad et al., 2014; Sahoo & Behera, 2019).

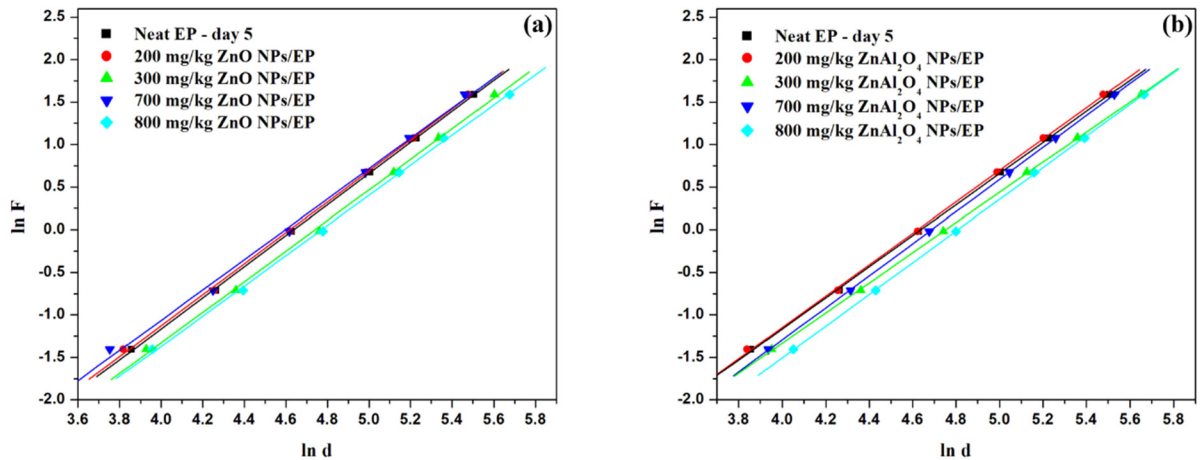


Figure 14. Variation of  $\ln F$  versus  $\ln d$  for EP coatings with and without (a) ZnO NPs and (b)  $ZnAl_2O_4$  NPs, on day 5

Table 3. Best fitting parameters according to Meyer's law

Sample	Concentration (mg/kg)	n	A × 10 <sup>-4</sup>
Neat EP		1.82	2.11
ZnO NPs	200	1.81	2.25
	300	1.79	1.99
	700	1.78	2.79
	800	1.77	2.12
ZnAl <sub>2</sub> O <sub>4</sub> NPs	200	1.84	2.00
	300	1.77	2.21
	700	1.88	1.47
	800	1.86	1.29

The normal ISE behavior of the EP coatings, with and without ZnO or ZnAl<sub>2</sub>O<sub>4</sub> nanoparticles, could be explained with Meyer's law, which is represented as (Awad et al., 2014; Sangwal, 2000):

$$F = A \times d^n \quad (6)$$

where  $A$  is a constant and  $n$  is Meyer's index (or number). Figures 14 (a) and (b) show  $\ln F$  versus  $\ln d$  for EP coatings, with and without ZnO or ZnAl<sub>2</sub>O<sub>4</sub> nanoparticles, respectively, on day 5. The values of  $n$  and  $A$  are listed in table 3. As seen,  $n$  values are less than 2 for all coatings, which confirms that  $H_v$  decreases with the increase in  $F$  and the samples exhibit normal ISE behavior (Awad et al., 2014; Sangwal, 2000). The other two cases,  $n > 2$  and  $n = 2$ , refer to reverse indentation size effect (RISE) behavior and  $H_v$  independent of  $F$ , respectively (Awad et al., 2014; Sangwal, 2000). Figure 12 (a-d) and Figure 13 (a-d) insets show that  $H_v$  has increased with 200 ZnO NPs/EP and 200 mg/kg ZnAl<sub>2</sub>O<sub>4</sub> NPs/EP, for all days, as compared to neat EP. Hardness is a parameter that expresses a material's resistance to deformation against a force concentrated on its surface (Bar, 2020). Thus, the addition of ZnO and ZnAl<sub>2</sub>O<sub>4</sub> nanoparticles was effective in improving the deformation resistance of EP coating. This may be attributed to the uniform dispersion of the ZnO and ZnAl<sub>2</sub>O<sub>4</sub> nanoparticles in the EP matrix, which limits the molecular chain mobility (Dass et al., 2017; Ozcan et al., 2019; Salahuddin et al., 2017). The high surface area of the nanoparticles reinforces a greater volume of the EP matrix and the load can be transferred to the fillers more efficiently due to the high interfacial area between the EP resin and the fillers. Hence, the material's resistance to deformation caused by the load increases (Dass et al., 2017; Ozcan et al., 2019; Salahuddin et al., 2017). A further increase in the concentration of ZnO NPs in EP to 700 mg/kg ZnO NPs/EP has further increased the  $H_v$  of EP coating. Nonetheless, a higher filler content ratio of 800 mg/kg ZnO NPs/EP showed a decrease in the  $H_v$  of the coating, as compared to neat EP. This might be due to the particles' agglomeration, which initiates cracks at the interfaces between the EP matrix and the nanofiller particles (Bisht et al., 2018; Dass et al., 2017). However, as compared to neat EP, the  $H_v$  values were declined with 300 mg/kg ZnO NPs/EP and 300 to 800 mg/kg ZnAl<sub>2</sub>O<sub>4</sub> NPs/EP samples. Scattering in  $H_v$  values may be due to the local positions exposed to the indenter on the surface of the coating sample, which might be free of nanoparticles, or with agglomerated or well-dispersed ZnO or ZnAl<sub>2</sub>O<sub>4</sub> nanoparticles (M et al., 2016; Muralishwara et al., 2020).

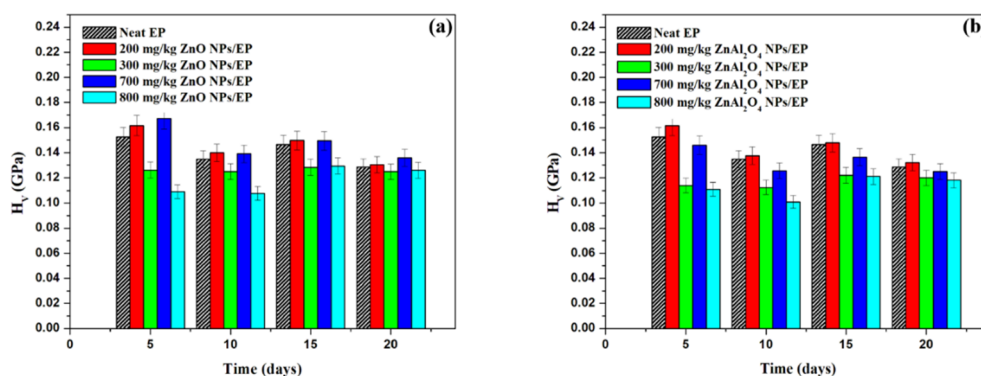


Figure 15. Variation of  $H_v$  with time for EP coatings with and without (a) ZnO NPs and (b) ZnAl<sub>2</sub>O<sub>4</sub> NPs, under 4.90 N

The effect of time on the  $H_v$  of neat EP, ZnO NPs/EP, and ZnAl<sub>2</sub>O<sub>4</sub> NPs/EP (200, 300, 700, and 800 mg/kg) coating samples, is shown in Figures 15 (a) and (b). As perceived, irrespective of the type of the nano-filler in EP, day 5 results show the highest  $H_v$  values for 200 ZnO NPs/EP, 700 mg/kg ZnO NPs/EP, and 200 mg/kg ZnAl<sub>2</sub>O<sub>4</sub> NPs/EP coatings. Subsequently, the  $H_v$  of the samples decreased, which may be attributed to the effect of the environmental conditions experienced by the reinforced EP coating samples (Glaskova-Kuzmina et al., 2020). The  $H_v$  values for neat EP, 200 mg/kg ZnO NPs/EP, 700 mg/kg ZnO NPs/EP, and 200 mg/kg ZnAl<sub>2</sub>O<sub>4</sub> NPs/EP samples were 0.153, 0.161, 0.167, and 0.162 GPa, respectively, on day 5. Thus, the improvements in the  $H_v$  of EP coating were 5.23, 9.15, and 5.88%, attained with 200 mg/kg ZnO NPs/EP, 700 mg/kg ZnO NPs/EP, and 200 mg/kg ZnAl<sub>2</sub>O<sub>4</sub> NPs/EP, respectively, as compared to neat EP. Figure 16 (a-c) shows indentations of neat EP, 300 mg/kg ZnO NPs/EP, and 200 mg/kg ZnAl<sub>2</sub>O<sub>4</sub> NPs/EP, respectively, under a 0.49 N load at dwell loading time of 30 seconds.

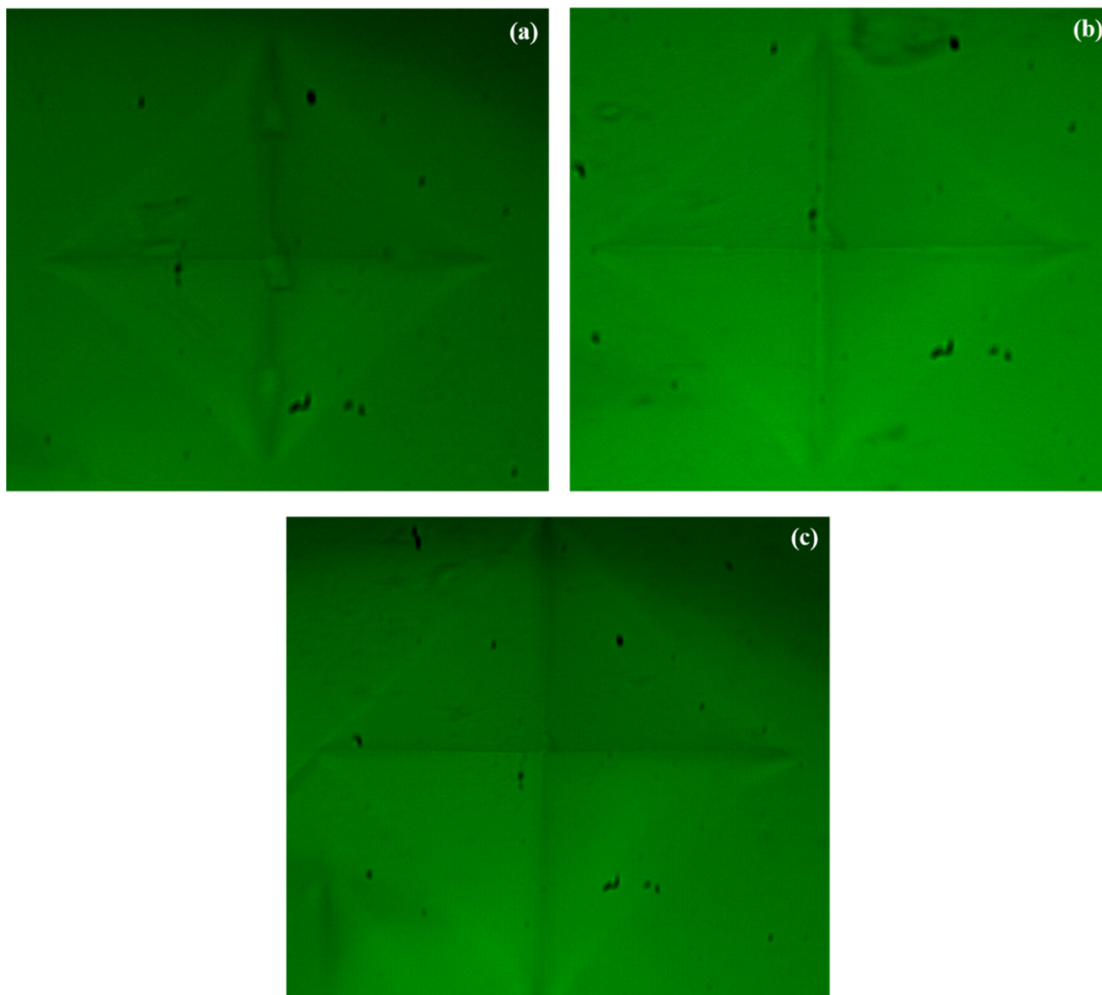


Figure 16. Typical indentations of (a) Neat EP, (b) 300 mg/kg ZnO NPs/EP, and (c) 200 mg/kg ZnAl<sub>2</sub>O<sub>4</sub> NPs/EP

#### 4. Conclusions

In this work, synthesized ZnO and ZnAl<sub>2</sub>O<sub>4</sub> NPs nanoparticles, via co-precipitation method, were incorporated into EP coating in concentrations 200, 300, 700, and 800 mg/kg of nanoparticles/EP. The mechanical properties of the coatings were investigated after 5, 10, 15, and 20 days of preparation. The results showed an enhancement in the tensile properties of EP coating upon the incorporation of ZnO and ZnAl<sub>2</sub>O<sub>4</sub> nanoparticles, in which the best improvement in the UTS of ZnO NPs/EP and ZnAl<sub>2</sub>O<sub>4</sub> NPs/EP coatings was reached on day 10 and day 15, respectively. The highest increase in UTS, by 93.2%, was attained with 800 mg/kg ZnAl<sub>2</sub>O<sub>4</sub> NPs/EP coating, as compared to neat EP. Moreover, the stress-strain curves revealed that all coatings showed brittle behavior. All specimens were rate sensitive, in which the UTS and Young's modulus have decreased with the decrease in the stretching rate from 3 to 1 mm/min. Particularly, ZnO NPs/EP coatings were more rate-sensitive than ZnAl<sub>2</sub>O<sub>4</sub> NPs/EP coatings. On the other hand, all EP coatings, with and without ZnO or ZnAl<sub>2</sub>O<sub>4</sub> nanoparticles, showed normal ISE behavior in Vickers microhardness tests. Vickers microhardness showed the best improvement on

day 5 with ZnO NPs/EP (200 and 700 mg/kg) and ZnAl<sub>2</sub>O<sub>4</sub>NPs/EP (200 mg/kg) coatings, as compared to neat EP. The maximum improvement in the  $H_v$  of EP coating was 9.15%, which was attained with 700 mg/kg ZnO NPs/EP coating. Finally, an EP coating containing ZnAl<sub>2</sub>O<sub>4</sub>NPs is recommended to achieve better mechanical properties. It might be worthy to further explore the effect of ZnO and ZnAl<sub>2</sub>O<sub>4</sub> nanoparticles on the mechanical properties of different coatings.

### Acknowledgements

Mechanical tests were performed in the Materials Science Laboratory, Beirut Arab University, Lebanon. The epoxy resin and its hardener were provided by Tinol Industries, Lebanon.

### References

- Adesina, A. Y., Zainelabdeen, I. H., Dalhat, M. A., Mohammed, A. S., Sorour, A. A., & Al-Badour, F. A. (2020). Influence of micronized waste tire rubber on the mechanical and tribological properties of epoxy composite coatings. *Tribology International*, *146*, 106244. <https://doi.org/10.1016/j.triboint.2020.106244>
- Al Boukhari, J., Zeidan, L., Khalaf, A., & Awad, R. (2019). Synthesis, characterization, optical and magnetic properties of pure and Mn, Fe and Zn doped NiO nanoparticles. *Chemical Physics*, *516*, 116-124. <https://doi.org/10.1016/j.chemphys.2018.07.046>
- Alsaad, A. M., Ahmad, A. A., Al-Bataineh, Q. M., Bani-Salameh, A. A., Abdullah, H. S., Qattan, I. A., Albataineh, Z. M., & Telfah, A. D. (2020). Optical, Structural, and Crystal Defects Characterizations of Dip Synthesized (Fe-Ni) Co-Doped ZnO Thin Films. *Materials*, *13*(7), 1737. <https://doi.org/10.3390/ma13071737>
- Alsayed, Z., Awad, R., & Badawi, M. S. (2020). Thermo-mechanical properties of high density polyethylene with zinc oxide as a filler. *Iranian Polymer Journal*, *29*(4), 309-320. <https://doi.org/10.1007/s13726-020-00796-7>
- Ammar, Sh., Ramesh, K., Vengadaesvaran, B., Ramesh, S., & Arof, A. K. (2016). Amelioration of anticorrosion and hydrophobic properties of epoxy/PDMS composite coatings containing nano ZnO particles. *Progress in Organic Coatings*, *92*, 54-65. <https://doi.org/10.1016/j.porgcoat.2015.12.007>
- Andrade, A. B., Ferreira, N. S., & Valerio, M. E. G. (2017). Particle size effects on structural and optical properties of BaF<sub>2</sub> nanoparticles. *RSC Advances*, *7*(43), 26839-26848. <https://doi.org/10.1039/C7RA01582H>
- Ariffin, M. M., Aung, M. M., Abdullah, L. C., & Salleh, M. Z. (2020). Assessment of corrosion protection and performance of bio-based polyurethane acrylate incorporated with nano zinc oxide coating. *Polymer Testing*, *87*, 106526. <https://doi.org/10.1016/j.polymertesting.2020.106526>
- Ashraf, M. A., Peng, W., Zare, Y., & Rhee, K. Y. (2018). Effects of Size and Aggregation/Agglomeration of Nanoparticles on the Interfacial/Interphase Properties and Tensile Strength of Polymer Nanocomposites. *Nanoscale Research Letters*, *13*(1), 214. <https://doi.org/10.1186/s11671-018-2624-0>
- Awad, R., Abou Aly, A. I., Mohammed, N. H., Isber, S., Motaweh, H. A., & El-Said Bakeer, D. (2014). Investigation on superconducting properties of GdBa<sub>2</sub>Cu<sub>3</sub>O<sub>7-δ</sub> added with nanosized ZnFe<sub>2</sub>O<sub>4</sub>. *Journal of Alloys and Compounds*, *610*, 614-622. <https://doi.org/10.1016/j.jallcom.2014.05.005>
- Babu, L. K., Sarala, E., Audisheshaiah, O., Reddy, K. M., & Reddy, Y. V. R. (2019). Synthesis, characterization of nanocrystalline ZnO via two different chemical methods and its antibacterial activity. *Surfaces and Interfaces*, *16*, 93-100. <https://doi.org/10.1016/j.surfin.2019.05.002>
- Baghdadi, Y. N., Youssef, L., Bouhadir, K., Harb, M., Mustapha, S., Patra, D., & Tehrani-Bagha, A. R. (2020). The effects of modified zinc oxide nanoparticles on the mechanical/thermal properties of epoxy resin. *Journal of Applied Polymer Science*, *137*(43), 49330. <https://doi.org/10.1002/app.49330>
- Bar, A. K. (2020). Chapter 5—Mechanical properties of oxide glassy nanocomposites. In S. Bhattacharya (Ed.), *Metal Oxide Glass Nanocomposites* (pp. 79-136). Elsevier. <https://doi.org/10.1016/B978-0-12-817458-6.00005-6>
- Bayal, N., & Jeevanandam, P. (2012). Synthesis of metal aluminate nanoparticles by sol-gel method and studies on their reactivity. *Journal of Alloys and Compounds*, *516*, 27-32. <https://doi.org/10.1016/j.jallcom.2011.11.080>

- Bazrgari, D., Moztarzadeh, F., Sabbagh-Alvani, A. A., Rasoulboroujeni, M., Tahriri, M., & Tayebi, L. (2018). Mechanical properties and tribological performance of epoxy/Al<sub>2</sub>O<sub>3</sub> nanocomposite. *Ceramics International*, 44(1), 1220-1224. <https://doi.org/10.1016/j.ceramint.2017.10.068>
- Belyaev, A. V., Lelet, M. I., Kirillova, N. I., Khamaletdinova, N. M., Boldin, M. S., Murashov, A. A., & Balabanov, S. S. (2019). Sol-gel synthesis and characterization of ZnAl<sub>2</sub>O<sub>4</sub> powders for transparent ceramics. *Ceramics International*, 45(4), 4835-4839. <https://doi.org/10.1016/j.ceramint.2018.11.179>
- Bisht, A., Dasgupta, K., & Lahiri, D. (2018). Effect of graphene and CNT reinforcement on mechanical and thermomechanical behavior of epoxy—A comparative study. *Journal of Applied Polymer Science*, 135(14), 46101. <https://doi.org/10.1002/app.46101>
- Dass, K., Chauhan, S. R., & Gaur, B. (2017). Study on the effects of nanoparticulates of SiC, Al<sub>2</sub>O<sub>3</sub>, and ZnO on the mechanical and tribological performance of epoxy-based nanocomposites. *Particulate Science and Technology*, 35(5), 589-606. <https://doi.org/10.1080/02726351.2016.1184730>
- Devaraju, A., Sivasamy, P., & Loganathan, G. B. (2020). Mechanical properties of polymer composites with ZnO nano-particle. *Materials Today: Proceedings*, 22, 531-534. <https://doi.org/10.1016/j.matpr.2019.08.146>
- Djafari Petroudy, S. R. (2017). 3—Physical and mechanical properties of natural fibers. In M. Fan & F. Fu (Eds.), *Advanced High Strength Natural Fibre Composites in Construction* (pp. 59-83). Woodhead Publishing. <https://doi.org/10.1016/B978-0-08-100411-1.00003-0>
- El-Fadl, A. A., Abd-Elrahman, M. I., Younis, N., Afify, N., Abu-Sehly, A. A., & Hafiz, M. M. (2019). Syntheses of new spinels Zn<sub>1-x</sub>FexAl<sub>2</sub>O<sub>4</sub> nanocrystallines structure: Optical and magnetic characteristics. *Journal of Alloys and Compounds*, 795, 114-119. <https://doi.org/10.1016/j.jallcom.2019.05.008>
- Fernández-Pérez, A., Rodríguez-Casado, V., Valdés-Solís, T., & Marbán, G. (2017). Room temperature sintering of polar ZnO nanosheets: II-mechanism. *Physical Chemistry Chemical Physics*, 19(25), 16413-16425. <https://doi.org/10.1039/C7CP02307C>
- Frigione, M., & Lettieri, M. (2020). Recent Advances and Trends of Nanofilled/Nanostructured Epoxies. *Materials*, 13(15), 3415. <https://doi.org/10.3390/ma13153415>
- Fu, S.-Y., Feng, X.-Q., Lauke, B., & Mai, Y.-W. (2008). Effects of particle size, particle/matrix interface adhesion and particle loading on mechanical properties of particulate-polymer composites. *Composites Part B: Engineering*, 39(6), 933-961. <https://doi.org/10.1016/j.compositesb.2008.01.002>
- Fukuhara, M. (2003). Lattice expansion of nanoscale compound particles. *Physics Letters A*, 313(5), 427-430. [https://doi.org/10.1016/S0375-9601\(03\)00793-X](https://doi.org/10.1016/S0375-9601(03)00793-X)
- Gallegos, M. V., Luna, C. R., Peluso, M. A., Damonte, L. C., Sambeth, J. E., & Jasen, P. V. (2019). Effect of Mn in ZnO using DFT calculations: Magnetic and electronic changes. *Journal of Alloys and Compounds*, 795, 254-260. <https://doi.org/10.1016/j.jallcom.2019.05.044>
- Galsin, J. S. (2019). Chapter 1—Crystal Structure of Solids. In J. S. Galsin (Ed.), *Solid State Physics* (pp. 1-36). Academic Press. <https://doi.org/10.1016/B978-0-12-817103-5.00001-3>
- Ghouch, N. E., Al-Oweini, R., & Awad, R. (2019). Synthesis, characterization and electrical properties of hybrid mono-iron-substituted undecatungstosilicate/(Bi,Pb)-2223 phase superconductors. *Materials Research Express*, 6(11), 116001. <https://doi.org/10.1088/2053-1591/ab46e2>
- Glaskova-Kuzmina, T., Aniskevich, A., Papanicolaou, G., Portan, D., Zotti, A., Borriello, A., & Zarrelli, M. (2020). Hydrothermal Aging of an Epoxy Resin Filled with Carbon Nanofillers. *Polymers*, 12(5), 1153. <https://doi.org/10.3390/polym12051153>
- Guo, X., Yin, P., Lei, W., Yang, H., Kanamori, K., & Nakanishi, K. (2017). Synthesis and characterization of monolithic ZnAl<sub>2</sub>O<sub>4</sub> spinel with well-defined hierarchical pore structures via a sol-gel route. *Journal of Alloys and Compounds*, 727, 763-770. <https://doi.org/10.1016/j.jallcom.2017.08.172>
- Gurusideswar, S., Srinivasan, N., Velmurugan, R., & Gupta, N. K. (2017). Tensile Response of Epoxy and Glass/Epoxy Composites at Low and Medium Strain Rate Regimes. *Procedia Engineering*, 173, 686-693. <https://doi.org/10.1016/j.proeng.2016.12.148>
- Han, D. (2017). Low-temperature synthesis and photoluminescence properties of oriented ZnAl<sub>2</sub>O<sub>4</sub> nanowire arrays. *Superlattices and Microstructures*, 111, 1093-1098. <https://doi.org/10.1016/j.spmi.2017.08.012>

- Hassan, N., Shahat, A., El-Didamony, A., El-Desouky, M. G., & El-Bindary, A. A. (2020). Synthesis and characterization of ZnO nanoparticles via zeolitic imidazolate framework-8 and its application for removal of dyes. *Journal of Molecular Structure*, 1210, 128029. <https://doi.org/10.1016/j.molstruc.2020.128029>
- Jagadeeshwaran, C., & Murugaraj, R. (2019). Impact of the sintering temperature on the structural, optical and electrical properties of zinc aluminate. *Journal of Materials Science: Materials in Electronics*, 30(16), 15683-15692. <https://doi.org/10.1007/s10854-019-01951-4>
- Jain, M., Manju, Gundimeda, A., Kumar, A., Kumar, S., Gupta, G., Won, S. O., Chae, K. H., Vij, A., & Thakur, A. (2019). Enhanced near-infrared luminescence in zinc aluminate bestowed by fuel-blended combustion approach. *Journal of Alloys and Compounds*, 797, 148-158. <https://doi.org/10.1016/j.jallcom.2019.04.257>
- Jensen, H., Pedersen, J. H., Jørgensen, J. E., Pedersen, J. S., Joensen, K. D., Iversen, S. B., & Søgaard, E. G. (2006). Determination of size distributions in nanosized powders by TEM, XRD, and SAXS. *Journal of Experimental Nanoscience*, 1(3), 355-373. <https://doi.org/10.1080/17458080600752482>
- Kamareddine, F., Boukhari, J. A., & Awad, R. (2020). Optoelectronic investigations of needle-shaped Zn<sub>1-x</sub>Sn<sub>x</sub>O nanoparticles synthesized by coprecipitation method. *Physica Scripta*, 95(10), 105804. <https://doi.org/10.1088/1402-4896/abb4f7>
- Kameswara Reddy, M., Suresh Babu, V., Sai Srinadh, K. V., & Bhargav, M. (2020). Mechanical properties of tungsten carbide nanoparticles filled epoxy polymer nano composites. *Materials Today: Proceedings*, 26, 2711-2713. <https://doi.org/10.1016/j.matpr.2020.02.569>
- Kibasomba, P. M., Dhlamini, S., Maaza, M., Liu, C.-P., Rashad, M. M., Rayan, D. A., & Mwakikunga, B. W. (2018). Strain and grain size of TiO<sub>2</sub> nanoparticles from TEM, Raman spectroscopy and XRD: The revisiting of the Williamson-Hall plot method. *Results in Physics*, 9, 628-635. <https://doi.org/10.1016/j.rinp.2018.03.008>
- Kumar, K., Ghosh, P. K., & Kumar, A. (2016). Improving mechanical and thermal properties of TiO<sub>2</sub>-epoxy nanocomposite. *Composites Part B: Engineering*, 97, 353-360. <https://doi.org/10.1016/j.compositesb.2016.04.080>
- Liu, J., Pang, M., Cao, G., Qu, G., Wang, X., Zhang, Y., Liu, R., & Shen, H. (2020). Comparative study of tensile properties and magnetic properties for Nb-doped Fe-based wires. *Journal of Materials Research and Technology*, 9(6), 12907-12916. <https://doi.org/10.1016/j.jmrt.2020.09.004>
- Liu, X., Chen, X., Ren, J., Chang, M., He, B., & Zhang, C. (2019). Effects of nano-ZnO and nano-SiO<sub>2</sub> particles on properties of PVA/xylan composite films. *International Journal of Biological Macromolecules*, 132, 978-986. <https://doi.org/10.1016/j.ijbiomac.2019.03.088>
- Lopes de Almeida, W., Ferreira, N. S., Rodembusch, F. S., & Caldas de Sousa, V. (2021). Study of structural and optical properties of ZnO nanoparticles synthesized by an eco-friendly tapioca-assisted route. *Materials Chemistry and Physics*, 258, 123926. <https://doi.org/10.1016/j.matchemphys.2020.123926>
- M, C. M., Rojas, D., Flores, P., Pérez-Tijerina, E., & Meléndrez, M. F. (2016). Effect of ZnO nanoparticles obtained by arc discharge on thermo-mechanical properties of matrix thermoset nanocomposites. *Journal of Applied Polymer Science*, 133(30). <https://doi.org/10.1002/app.43631>
- Ma, X., Peng, C., Zhou, D., Wu, Z., Li, S., Wang, J., & Sun, N. (2018). Synthesis and mechanical properties of the epoxy resin composites filled with sol-gel derived ZrO<sub>2</sub> nanoparticles. *Journal of Sol-Gel Science and Technology*, 88(2), 442-453. <https://doi.org/10.1007/s10971-018-4827-3>
- Mahamuni, P. P., Patil, P. M., Dhanavade, M. J., Badiger, M. V., Shadija, P. G., Lokhande, A. C., & Bohara, R. A. (2019). Synthesis and characterization of zinc oxide nanoparticles by using polyol chemistry for their antimicrobial and antibiofilm activity. *Biochemistry and Biophysics Reports*, 17, 71-80. <https://doi.org/10.1016/j.bbrep.2018.11.007>
- Multian, V. V., Uklein, A. V., Zaderko, A. N., Kozhanov, V. O., Boldyrieva, O. Y., Linnik, R. P., Lisnyak, V. V., & Gayvoronsky, V. Y. (2017). Synthesis, Characterization, Luminescent and Nonlinear Optical Responses of Nanosized ZnO. *Nanoscale Research Letters*, 12(1), 164. <https://doi.org/10.1186/s11671-017-1934-y>
- Muñoz-Hernández, G., Escobedo-Morales, A., & Pal, U. (2009). Thermolytic Growth of ZnO Nanocrystals: Morphology Control and Optical Properties. *Crystal Growth & Design*, 9(1), 297-300. <https://doi.org/10.1021/cg8004807>

- Muralishwara, K., Kini, U. A., & Sharma, S. (2020). Surface properties of epoxy clay nanocomposite coating. *Materials Today: Proceedings*. <https://doi.org/10.1016/j.matpr.2020.08.534>
- Naik, E. I., Naik, H. S. B., Viswanath, R., Kirthan, B. R., & Prabhakara, M. C. (2020). Effect of zirconium doping on the structural, optical, electrochemical and antibacterial properties of ZnO nanoparticles prepared by sol-gel method. *Chemical Data Collections*, 29, 100505. <https://doi.org/10.1016/j.cdc.2020.100505>
- Nguyen, T. A., Nguyen, T. H., Nguyen, T. V., Thai, H., & Shi, X. (2016). Effect of Nanoparticles on the Thermal and Mechanical Properties of Epoxy Coatings. *Journal of Nanoscience and Nanotechnology*, 16(9), 9874-9881. <https://doi.org/10.1166/jnn.2016.12162>
- Nikolic, G., Zlatkovic, S., Cakic, M., Cakic, S., Lacnjevac, C., & Rajic, Z. (2010). Fast Fourier transform IR characterization of epoxy GY systems crosslinked with aliphatic and cycloaliphatic EH polyamine adducts. *Sensors*, 10(1), 684-696. <https://doi.org/10.3390/s100100684>
- Odegard, G. M., & Bandyopadhyay, A. (2011). Physical aging of epoxy polymers and their composites. *Journal of Polymer Science Part B: Polymer Physics*, 49(24), 1695-1716. <https://doi.org/10.1002/polb.22384>
- Ozcan, U. E., Karabork, F., Yazman, S., & Akdemir, A. (2019). Effect of Silica/Graphene Nanohybrid Particles on the Mechanical Properties of Epoxy Coatings. *Arabian Journal for Science and Engineering*, 44(6), 5723-5731. <https://doi.org/10.1007/s13369-019-03724-x>
- Pattanaik, A., Mukharjee, M., & Mishra, S. C. (2020). Effect of environmental aging conditions on the properties of fly ash filled epoxy composites. *Advanced Composite Materials*, 29(1), 1-30. <https://doi.org/10.1080/09243046.2019.1610930>
- Rahman, R., & Zhafer Firdaus Syed Putra, S. (2019). 5—Tensile properties of natural and synthetic fiber-reinforced polymer composites. In M. Jawaid, M. Thariq & N. Saba (Eds.), *Mechanical and Physical Testing of Biocomposites, Fibre-Reinforced Composites and Hybrid Composites* (pp. 81-102). Woodhead Publishing. <https://doi.org/10.1016/B978-0-08-102292-4.00005-9>
- Saba, N., Alothman, O. Y., Almutairi, Z., Jawaid, M., & Ghori, W. (2019). Date palm reinforced epoxy composites: Tensile, impact and morphological properties. *Journal of Materials Research and Technology*, 8(5), 3959-3969. <https://doi.org/10.1016/j.jmrt.2019.07.004>
- Sahoo, B., & Behera, D. (2019). Investigation of superconducting and elastic parameters of YBCO/LSMO thick films. *Journal of Materials Science: Materials in Electronics*, 30(14), 12992-13004. <https://doi.org/10.1007/s10854-019-01661-x>
- Salahuddin, N. A., El-Kemary, M., & Ibrahim, E. M. (2017). High-performance flexible epoxy/ZnO nanocomposites with enhanced mechanical and thermal properties. *Polymer Engineering & Science*, 57(9), 932-946. <https://doi.org/10.1002/pen.24520>
- Samad, U. A., Alam, M. A., Chafidz, A., Al-Zahrani, S. M., & Alharthi, N. H. (2018). Enhancing mechanical properties of epoxy/polyaniline coating with addition of ZnO nanoparticles: Nanoindentation characterization. *Progress in Organic Coatings*, 119, 109-115. <https://doi.org/10.1016/j.porgcoat.2018.02.018>
- Sameera, S., Vidyadharan, V., Sasidharan, S., & Gopchandran, K. G. (2019). Nanostructured zinc aluminates: A promising material for cool roof coating. *Journal of Science: Advanced Materials and Devices*, 4(4), 524-530. <https://doi.org/10.1016/j.jsamd.2019.10.003>
- Sangwal, K. (2000). On the reverse indentation size effect and microhardness measurement of solids. *Materials Chemistry and Physics*, 63(2), 145-152. [https://doi.org/10.1016/S0254-0584\(99\)00216-3](https://doi.org/10.1016/S0254-0584(99)00216-3)
- Savvilotidou, M., Vassilopoulos, A. P., Frigione, M., & Keller, T. (2017). Effects of aging in dry environment on physical and mechanical properties of a cold-curing structural epoxy adhesive for bridge construction. *Construction and Building Materials*, 140, 552-561. <https://doi.org/10.1016/j.conbuildmat.2017.02.063>
- Shaban, M., Hosny, R., Rabie, A. M., Shim, J.-J., Ahmed, S. A., Betiha, M. A., & Negm, N. A. (2020). Zinc aluminate nanoparticles: Preparation, characterization and application as efficient and economic catalyst in transformation of waste cooking oil into biodiesel. *Journal of Molecular Liquids*, 302, 112377. <https://doi.org/10.1016/j.molliq.2019.112377>
- Shen, W., Zhang, T., Ge, Y., Feng, L., Feng, H., & Li, P. (2021). Multifunctional AgO/epoxy nanocomposites with enhanced mechanical, anticorrosion and bactericidal properties. *Progress in Organic Coatings*, 152, 106130. <https://doi.org/10.1016/j.porgcoat.2020.106130>

- Shi, X., Nguyen, T. A., Suo, Z., Liu, Y., & Avci, R. (2009). Effect of nanoparticles on the anticorrosion and mechanical properties of epoxy coating. *Surface and Coatings Technology*, 204(3), 237-245. <https://doi.org/10.1016/j.surfcoat.2009.06.048>
- Shmait, A., Awad, R., Rahal, H. T., Azouri, M., & Abdel-Gaber, A. M. (n.d.). Studies on coatings containing nano-zinc oxide for steel protection. *Materials and Corrosion*, 72(5), 859-867. <https://doi.org/10.1002/maco.202012010>
- Srouf, A., Malaeb, W., Rekaby, M., & Awad, R. (2017). Mechanical properties of the (BaSnO<sub>3</sub>)<sub>x</sub>/Cu<sub>0.5</sub>Tl<sub>0.5</sub>Ba<sub>2</sub>Ca<sub>2</sub>Cu<sub>3</sub>O<sub>10-δ</sub> superconductor phase. *Physica Scripta*, 92(10), 104002. <https://doi.org/10.1088/1402-4896/aa86ce>
- Staszak, W., Zawadzki, M., & Okal, J. (2010). Solvothermal synthesis and characterization of nanosized zinc aluminate spinel used in iso-butane combustion. *Journal of Alloys and Compounds*, 492(1), 500-507. <https://doi.org/10.1016/j.jallcom.2009.11.151>
- Stringhini, F. M., Foletto, E. L., Sallet, D., Bertuol, D. A., Chiavone-Filho, O., & Nascimento, C. A. O. do. (2014). Synthesis of porous zinc aluminate spinel (ZnAl<sub>2</sub>O<sub>4</sub>) by metal-chitosan complexation method. *Journal of Alloys and Compounds*, 588, 305-309. <https://doi.org/10.1016/j.jallcom.2013.11.078>
- Sturdy, L. F., Wright, M. S., Yee, A., Casadio, F., Faber, K. T., & Shull, K. R. (2020). Effects of zinc oxide filler on the curing and mechanical response of alkyd coatings. *Polymer*, 191, 122222. <https://doi.org/10.1016/j.polymer.2020.122222>
- Subhasree, S., Anitha, P., Kannan, K., Ramachandran, A., Sheri, J. J., & Jayavel, R. (2020). Anticorrosion Behavior of ZnO Nanoparticles Coated on Mild Steel in NaCl Solution. *Journal of Nanoscience and Nanotechnology*, 20(7), 4061-4068. <https://doi.org/10.1166/jnn.2020.17526>
- Suwanboon, S., Amornpitoksuk, P., Rattana, T., & Randorn, C. (2020). Investigation of g-C<sub>3</sub>N<sub>4</sub>/ZnAl<sub>2</sub>O<sub>4</sub> and ZnO/ZnAl<sub>2</sub>O<sub>4</sub> nanocomposites: From synthesis to photocatalytic activity of pollutant dye model. *Ceramics International*, 46(14), 21958-21977. <https://doi.org/10.1016/j.ceramint.2020.04.243>
- Tangcharoen, T., Klysubun, W., & Kongmark, C. (2019). Synchrotron X-ray absorption spectroscopy and cation distribution studies of NiAl<sub>2</sub>O<sub>4</sub>, CuAl<sub>2</sub>O<sub>4</sub>, and ZnAl<sub>2</sub>O<sub>4</sub> nanoparticles synthesized by sol-gel auto combustion method. *Journal of Molecular Structure*, 1182, 219-229. <https://doi.org/10.1016/j.molstruc.2019.01.049>
- Theophile, T. (2012). *Infrared Spectroscopy: Materials Science, Engineering and Technology*. BoD – Books on Demand.
- Tian, Q., Ran, M., Fang, G., Ding, L., Pan, A., Shen, K., & Deng, Y. (2020). ZnAl<sub>2</sub>O<sub>4</sub>/BiPO<sub>4</sub> composites as a heterogeneous catalyst for photo-Fenton treatment of textile and pulping wastewater. *Separation and Purification Technology*, 239, 116574. <https://doi.org/10.1016/j.seppur.2020.116574>
- Tsai, M.-T., Chang, Y.-S., Huang, I.-B., & Pan, B.-Y. (2013). Luminescent and structural properties of manganese-doped zinc aluminate spinel nanocrystals. *Ceramics International*, 39(4), 3691-3697. <https://doi.org/10.1016/j.ceramint.2012.10.201>
- Ünal, M., Akkuş, O., & Marcus, R. E. (2016). Fundamentals of Musculoskeletal Biomechanics. In F. Korkusuz (Ed.), *Musculoskeletal Research and Basic Science* (pp. 15-36). Springer International Publishing. [https://doi.org/10.1007/978-3-319-20777-3\\_2](https://doi.org/10.1007/978-3-319-20777-3_2)
- Verma, S., Das, S., Mohanty, S., & Nayak, S. K. (2019). Development of multifunctional polydimethylsiloxane (PDMS)-epoxy-zinc oxide nanocomposite coatings for marine applications. *Polymers for Advanced Technologies*, 30(9), 2275-2300. <https://doi.org/10.1002/pat.4656>
- Vijayakumar, S., Arulmozhi, P., Kumar, N., Sakthivel, B., Prathip Kumar, S., & Praseetha, P. K. (2020). Acalypha fruticosa L. leaf extract mediated synthesis of ZnO nanoparticles: Characterization and antimicrobial activities. *Materials Today: Proceedings*, 23, 73-80. <https://doi.org/10.1016/j.matpr.2019.06.660>
- Vu, T. V., Nguyen, T. V., Tabish, M., Ibrahim, S., Hoang, T. H. T., Gupta, R. K., Dang, T. M. L., Nguyen, T. A., & Yasin, G. (2021). Water-Borne ZnO/Acrylic Nanocoating: Fabrication, Characterization, and Properties. *Polymers*, 13(5), 717. <https://doi.org/10.3390/polym13050717>

- Wang, X., Tang, F., Qi, X., & Lin, Z. (2019). Mechanical, electrochemical, and durability behavior of graphene nano-platelet loaded epoxy-resin composite coatings. *Composites Part B: Engineering*, *176*, 107103. <https://doi.org/10.1016/j.compositesb.2019.107103>
- Wei, L., Chen, X., Hong, K., Yuan, Z., Wang, L., Wang, H., Qiao, Z., Wang, X., Li, Z., & Wang, Z. (2019). Enhancement in mechanical properties of epoxy nanocomposites by Styrene-ethylene-butadiene-styrene grafted graphene oxide. *Composite Interfaces*, *26*(2), 141-156. <https://doi.org/10.1080/09276440.2018.1481303>
- Wetzel, B., Hauptert, F., & Qiu Zhang, M. (2003). Epoxy nanocomposites with high mechanical and tribological performance. *Composites Science and Technology*, *63*(14), 2055-2067. [https://doi.org/10.1016/S0266-3538\(03\)00115-5](https://doi.org/10.1016/S0266-3538(03)00115-5)
- Wu, M., Lu, L., Yu, L., Yu, X., Naito, K., Qu, X., & Zhang, Q. (2020). Preparation and Characterization of Epoxy/Alumina Nanocomposites. *Journal of Nanoscience and Nanotechnology*, *20*(5), 2964-2970. <https://doi.org/10.1166/jnn.2020.17460>
- Wu, Y., Wu, X., Yang, F., & Ye, J. (2020). Preparation and Characterization of Waterborne UV Lacquer Product Modified by Zinc Oxide with Flower Shape. *Polymers*, *12*, 668. <https://doi.org/10.3390/polym12030668>
- Xia, Y., He, Y., Chen, C., Wu, Y., & Chen, J. (2019). MoS<sub>2</sub> nanosheets modified SiO<sub>2</sub> to enhance the anticorrosive and mechanical performance of epoxy coating. *Progress in Organic Coatings*, *132*, 316-327. <https://doi.org/10.1016/j.porgcoat.2019.04.002>
- Xiao, C., Tan, Y., Yang, X., Xu, T., Wang, L., & Qi, Z. (2018). Mechanical properties and strengthening mechanism of epoxy resin reinforced with nano-SiO<sub>2</sub> particles and multi-walled carbon nanotubes. *Chemical Physics Letters*, *695*, 34-43. <https://doi.org/10.1016/j.cpllett.2018.01.060>
- Xing, S., Song, S., & Xiang, J. (2020). Low temperature combustion synthesis and photoluminescence mechanism of ZnO/ZnAl<sub>2</sub>O<sub>4</sub> composite phosphors. *Optik*, *208*, 164526. <https://doi.org/10.1016/j.ijleo.2020.164526>
- Xu, J., Song, R., Dai, Y., Yang, S., Li, J., & Wei, R. (2019). Characterization of zinc oxide nanoparticles-epoxy resin composite and its antibacterial effects on spoilage bacteria derived from silvery pomfret (*Pampus argenteus*). *Food Packaging and Shelf Life*, *22*, 100418. <https://doi.org/10.1016/j.fpsl.2019.100418>
- Yang, R., Han, A., Ye, M., Chen, X., & Yuan, L. (2017). The influence of Mn/N-codoping on the thermal performance of ZnAl<sub>2</sub>O<sub>4</sub> as high near-infrared reflective inorganic pigment. *Journal of Alloys and Compounds*, *696*, 1329-1341. <https://doi.org/10.1016/j.jallcom.2016.12.100>
- Yazman, Ş., & Samancı, A. (2019). A Comparative Study on the Effect of CNT or Alumina Nanoparticles on the Tensile Properties of Epoxy Nanocomposites. *Arabian Journal for Science and Engineering*, *44*(2), 1353-1363. <https://doi.org/10.1007/s13369-018-3516-4>
- Yu, M., Fan, C., Han, S., Ge, F., Cui, Z., Lu, Q., & Wang, X. (2020). Anticorrosion behavior of superhydrophobic particles reinforced epoxy coatings for long-time in the high salinity liquid. *Progress in Organic Coatings*, *147*, 105867. <https://doi.org/10.1016/j.porgcoat.2020.105867>
- Yuvasravana, R., George, P. P., & Devanna, N. (2017). Synthesis and characterization of spinel metal aluminate by a simple microwave assisted green synthesis. *Materials Today: Proceedings*, *4*(10), 10664-10671. <https://doi.org/10.1016/j.matpr.2017.08.012>
- Zak, A. K., Majid, W. H. Abd., Darroudi, M., & Yousefi, R. (2011). Synthesis and characterization of ZnO nanoparticles prepared in gelatin media. *Materials Letters*, *65*(1), 70-73. <https://doi.org/10.1016/j.matlet.2010.09.029>
- Zalaoglu, Y., Karaboga, F., Terzioglu, C., & Yildirim, G. (2017). Improvement of mechanical performances and characteristics of bulk Bi-2212 materials exposed to Au diffusion and stabilization of durable tetragonal phase by Au. *Ceramics International*, *43*(9), 6836-6844. <https://doi.org/10.1016/j.ceramint.2017.02.104>
- Zheng, Y., Chen, C., Zhan, Y., Lin, X., Zheng, Q., Wei, K., Zhu, J., & Zhu, Y. (2007). Luminescence and Photocatalytic Activity of ZnO Nanocrystals: Correlation between Structure and Property. *Inorganic Chemistry*, *46*(16), 6675-6682. <https://doi.org/10.1021/ic062394m>

### Copyrights

Copyright for this article is retained by the author(s), with first publication rights granted to the journal.

This is an open-access article distributed under the terms and conditions of the Creative Commons Attribution license (<http://creativecommons.org/licenses/by/4.0/>).